研究成果による特許権等の知的財産権の出願・登録状況

氏名	題名	番号	取得日
岩田　裕子、若林繁夫	TRPV2の部分ペプチド	特許第5644026号	平成26年11月14日
岩田　裕子、若林繁夫	TRPV2阻害剤、疾患の予防又は治療剤、薬剤探索用リード化合物、及び薬剤探索方法	特許第5667223号	平成26年12月19日

その他

発表内容	題名	年度
第 32 回全国筋ジストロフィー大阪大会 基調講演：　裏出　良博	デュシェンヌ型筋ジストロフィーの薬物療法	2014年10月
大鵬薬品工業㈱登録番号（NCT02246478）臨床試験開始 *米国 NIH 広報	H-PGDS阻害薬（TAS-205）を用いたDMD患者を対象とした臨床試験	2014年9月

nature neuroscience

Prostaglandin D2 synthase/GPR44: a signaling axis in PNS myelination

Amelia Trimarco[1,2], Maria Grazia Forese[1,2], Valentina Alfieri[1,2], Alessandra Lucente[1,2], Paola Brambilla[1,2], Giorgia Dina[1,2], Damiana Pieragostino[3], Paolo Sacchetta[3], Yoshihiro Urade[4], Brigitte Boizet-Bonhoure[5], Filippo Martinelli Boneschi[1,2], Angelo Quattrini[1,2] & Carla Taveggia[1,2]

Neuregulin 1 type III is processed following regulated intramembrane proteolysis, which allows communication from the plasma membrane to the nucleus. We found that the intracellular domain of neuregulin 1 type III upregulated the prostaglandin D2 synthase (*L-pgds*, also known as *Ptgds*) gene, which, together with the G protein–coupled receptor Gpr44, forms a previously unknown pathway in PNS myelination. Neuronal L-PGDS is secreted and produces the PGD2 prostanoid, a ligand of Gpr44. We found that mice lacking L-PGDS were hypomyelinated. Consistent with this, specific inhibition of L-PGDS activity impaired *in vitro* myelination and caused myelin damage. Furthermore, *in vivo* ablation and *in vitro* knockdown of glial Gpr44 impaired myelination. Finally, we identified Nfatc4, a key transcription factor for myelination, as one of the downstream effectors of PGD2 activity in Schwann cells. Thus, L-PGDS and Gpr44 are previously unknown components of an axo-glial interaction that controls PNS myelination and possibly myelin maintenance.

Glial cells, oligodendrocytes in the CNS and Schwann cells in the PNS, wrap around axons to form myelin, which is essential for rapid conduction of electrical impulses and neuronal survival. In the PNS, the levels of axonal neuregulin 1 (NRG1) type III, a member of the NRG family of growth factors, controls all aspects of Schwann cell development and myelin formation[1]. We recently found that NRG1 type III activity is modulated by competitive extracellular cleavage between the beta secretase BACE-1 (refs. 2,3) and the alpha secretase TACE (Adam17)[4].

NRG1 type III is also intramembrane processed by the γ-secretase complex following a classically regulated intramembrane proteolysis cleavage, suggesting that it might function as a bidirectional molecule[5]. Previous studies showed that, in hippocampal neurons, this cleavage event is regulated by the erbB receptors and generates an intracellular domain that represses the expression of pro-apoptotic genes *in vitro*[5]. In the mouse cochlea, the NRG1 intracellular domain can be further processed to generate a smaller fragment that enhances the expression of PSD95 (Dlg4)[6]. Finally, mutations in the putative transmembrane cleavage domain of NRG1 alter the branching of cortical dendrites[7].

We report that NRG1 type III undergoes a similar intramembrane processing in the PNS, but, unlike previous studies, we found that the generated fragment upregulated the prostaglandin D2 synthase (*L-pgds*) gene. L-PGDS, an *N*-glycosylated protein that is highly expressed in several tissues[8], is part of the prostaglandin synthase' family of proteins and controls many biological events. L-PGDS can be secreted[9,10] and functions as an enzyme or as an extracellular transporter of lipoliphic molecules[11]. Prostaglandins are generated by the processing of arachidonic acid and have been mainly implicated in inflammation. Following release by phospholipase A, arachidonic acid binds to the catalytic site of the COX enzymes (Cox-1 and Cox2) to generate the intermediate prostaglandin H2 (PGH2)[12,13]. Several synthases, including L-PGDS, convert this metabolite into different prostaglandins. L-PGDS catalyzes the conversion of PGH2 into the functional prostaglandin D2 (PGD2). PGD2 is also synthesized by the hematopoietic prostaglandin D synthase (*H-pgds*, also known as *Ptgds2*), which is expressed in inflammatory cells and in microglial cells[8]. PGD2 can be further dehydrated to PGJ2. 15d-PGJ2, the final non-enzymatic product of PGD2 dehydration, has a variety of biological actions, including neurotoxic and neuroprotective properties[13,14]. PGD2 and PGJ2 can bind Gpr44 and Ptgdr, members of the G protein–coupled receptor family, and the nuclear receptor Pparg[15], respectively. After binding, they activate intracellular signaling responses that vary depending on the type of receptor initially stimulated[16]. In particular, PGD2 modulates intracellular messengers such as calcium, cAMP and phosphoinositol concentrations[15,17].

We found that intracellular cleavage and nuclear translocation of NRG1 type III in the PNS induced the expression of L-PGDS and the activation of Gpr44, which contribute to myelin formation and maintenance. Inhibition of L-PGDS activity *in vitro* impaired PNS myelination. Accordingly, sciatic nerves of *L-pgds*$^{-/-}$ transgenic mice were hypomyelinated. We also found that H-PGDS was expressed in nerves, but was dispensable for myelination. Notably,

[1]Division of Neuroscience, San Raffaele Scientific Institute, Milan, Italy. [2]INSPE at San Raffaele Scientific Institute, Milan, Italy. [3]Department of Experimental and Clinical Sciences, University "G. D'Annunzio", Chieti, Italy. [4]International Institute for Integrative Sleep medicine, University of Tsukuba, Ibaraki, Japan. [5]Institut de Génétique Humaine CNRS UPR1142, Montpellier, France. Correspondence should be addressed to C.T. (taveggia.carla@hsr.it).

Received 23 July; accepted 7 October; published online 2 November 2014; corrected online 17 November 2014 (details online); doi:10.1038/nn.3857

H-pgds $^{-/-}$*; L-pgds*$^{-/-}$ mice were hypomyelinated and the myelin sheath was aberrant in aged animals. Furthermore, we found that PGD2, the product of L-PGDS enzymatic activity, most likely signals through the Gpr44 receptor onto Schwann cells, as glial-specific knockdown of Gpr44 impaired *in vitro* myelination. *Gpr44*$^{-/-}$ transgenic mice were hypomyelinated in the PNS. Finally, activation of Gpr44 led to dephosphorylation of the transcription factor Nfatc4 (ref. 18), indicating that it is a downstream effector of L-PGDS activity.

We propose that L-PGDS and the G protein–coupled receptor Gpr44 are modulators of PNS myelination. Our findings suggest that NRG1 type III controls myelination in multiple ways and our data support the existence of a previously unknown pathway whose modulation could be beneficial for the treatment of peripheral demyelinating neuropathies. To the best of our knowledge, these results are the first to implicate prostaglandins as active controllers of myelination.

RESULTS

NRG1 type III is cleaved by γ-secretase and activates L-PGDS

To investigate whether NRG1 type III intracellular cleavage occurs in PNS neurons, we generated two lentiviral vectors expressing NRG1 type III tagged with an EGFP epitope at either the N-terminal (N-NRG1) or C-terminal end (C-NRG1). We then infected rat primary dorsal root ganglia (DRG) neurons and found that N-NRG1 (data not shown) and C-NRG1 were similarly expressed in axons. However, C-NRG1 was no longer present following Schwann cell contact (**Fig. 1a**). Notably, addition of 10 μM γ-secretase specific inhibitor Compound E[19] maintained the expression of the EGFP epitope in the axons (**Fig. 1a**), suggesting that the C-terminal end of NRG1 type III undergoes a γ-secretase–dependent cleavage, which is also Schwann cell dependent.

To determine whether the generated NRG1 type III fragment translocates into the nucleus, we infected rat primary DRG neurons with a lentiviral construct expressing the constitutively cleaved form of NRG1 type III tagged with a FLAG epitope at the C terminus (NRG1 ICD). Immunofluorescence analyses revealed that the FLAG epitope was present in nuclei of DRG infected neurons (**Fig. 1b**). We observed NRG1 ICD staining in approximately 78% of DRG neurons, 66.2% ± 18.8 of which expressed nuclear FLAG (four different infections, at least three coverslips per infection).

Despite this result, the conditions of our experiment were not physiologically realistic due to the expression of the already processed fragment. Thus, to assess whether NRG1 ICD physiologically translocates, we infected DRG neurons with a lentivirus expressing full-length NRG1 type III tagged with a FLAG epitope at the C terminus. Our initial finding implicated Schwann cells in the intracellular processing of full-length NRG1 type III. Thus, 7 d after infection, we added rat primary Schwann cells to DRG neurons and we examined FLAG localization by immunofluorescence. As expected, we detected the FLAG epitope in the nuclei of infected DRG neurons (**Fig. 1c**), confirming that NRG1 type III physiologically undergoes classical intramembrane proteolysis.

To evaluate whether NRG1 ICD nuclear translocation modifies gene transcription, we performed genome-wide expression analysis on an Illumina platform. We compared mRNA expression levels of DRG

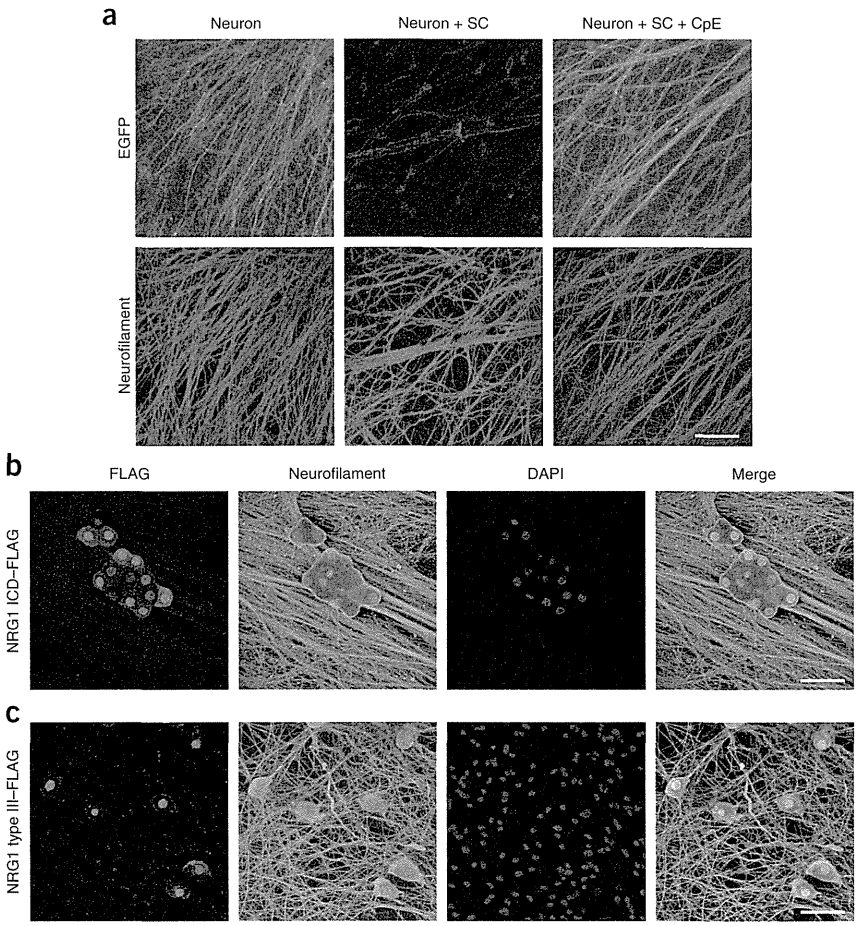

Figure 1 NRG1 type III undergoes a regulated intramembrane proteolysis cleavage that is Schwann cell dependent. (**a**) Rat DRG neurons infected with full-length NRG1 type III, tagged at the C terminus with EGFP, were stained for GFP (fluorescein) and neurofilament (rhodamine). The addition of Schwann cells induced clearance while in the presence of 10 μM Compound E (CpE). EGFP expression remained associated to the axons. The images are representative of three different independent experiments ($N = 3$ infections performed with different viral stock preparation onto different neuronal cultures). Scale bar represents 100 μm. (**b**) Rat DRG neurons were infected with a lentivirus expressing NRG1 ICD tagged with a FLAG epitope at the C terminus. The FLAG tag (rhodamine) was expressed in the nuclei, as shown by colocalization with nuclear staining (DAPI, blue). Neurofilament staining is also indicated (fluorescein). The images are representative of three different independent experiments ($N = 3$ infections performed with different viral stock preparation onto different neuronal cultures). Scale bar represents 100 μm. (**c**) Rat DRG neurons were infected with a lentivirus expressing full-length NRG1 type III tagged with a FLAG epitope at the C terminus. In the presence of Schwann cells, the FLAG tag (rhodamine) was expressed in the nuclei, as shown by colocalization with nuclear staining (DAPI, blue). Neurofilament staining is also indicated (fluorescein). The images are representative of three different independent experiments ($N = 3$ infections performed with different viral stock preparation onto different neuronal cultures). Scale bar represents 100 μm.

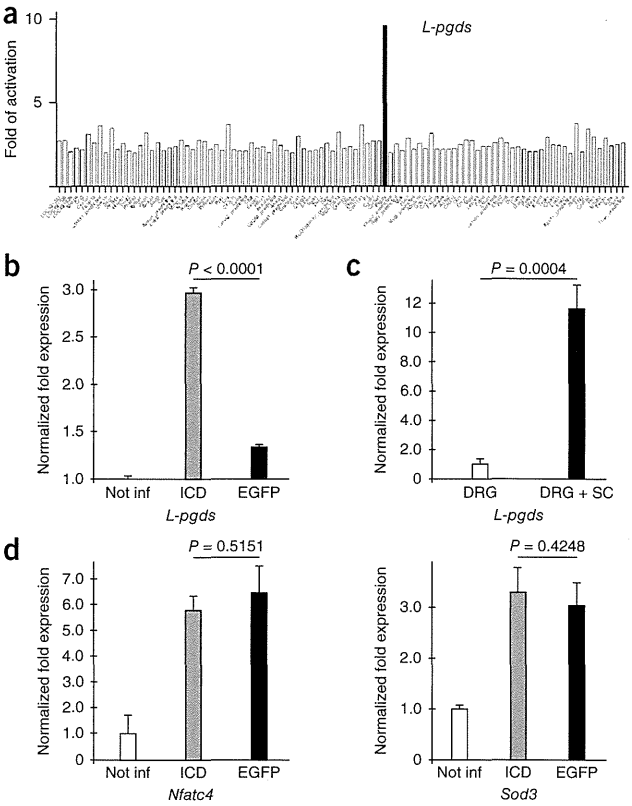

Figure 2 *L-pgds* is the most upregulated gene in neurons infected with NRG1 ICD. (**a**) Graph indicating all genes that were significantly upregulated in the Illumina analyses in NRG1 ICD–infected neurons compared with uninfected neurons. *L-pgds* showed a nine-fold change of activation (Limma moderated *t* test, $P = 0.00015$, $t = 5.25$, df = 6). $N = 4$ different independent RNA preparations and analyses. The complete list of upregulated genes is reported in **Supplementary Table 1**. (**b**) *L-PGDS* was upregulated only in neurons overexpressing NRG1 ICD. qRT-PCR analyses of mRNA prepared from DRG neurons not infected or infected with a lentivirus expressing either NRG1 ICD or EGFP confirmed specific upregulation of *L-pgds* in DRG neurons expressing NRG1 ICD. Data have been normalized to *Gapdh* expression level. Data were analyzed with the CFX Manager Software (Biorad) (one-way ANOVA, $***P \leq 0.0001$ NRG1 ICD versus EGFP (ICD – EGFP), $F = 706$). Error bars represent mean ± s.e.m. Graph is representative of three different independent experiments. $N = 3$ different RNA preparations and analyses. (**c**) Neuronal *L-PGDS* expression was upregulated in DRG neurons following the addition of Schwann cells. qRT-PCR analyses of mRNA prepared from purified mouse DRG neurons and mouse DRG neurons seeded with rat primary Schwann cells are shown. Amplification with primers specifically designed for mouse *L-pgds*, which do not amplify the rat *L-pgds* sequence, confirmed that neuronal *L-pgds* expression was induced by Schwann cell contact. Data are normalized to *Gapdh* expression level (*t* test analysis, $P = 0.0004$, $t = 10.8$, df = 4). Error bars represent mean ± s.d. Shown graph is representative of three different independent experiments. $N = 3$ different RNA preparations and analyses. (**d**) qRT-PCR analyses of mRNA prepared from DRG neurons not infected or infected with a lentivirus expressing either NRG1 ICD or EGFP to test the expression of genes that in the Illumina screening were upregulated above threshold. Upregulation of *Nfatc4* and *Sod3* was not specific, as it is also present in EGFP-infected DRG neurons. Data were analyzed with the CFX Manager Software on three mRNA different preparations (one-way ANOVA: *Sod3*, $P = 0.5151$ ICD – EGFP, $F = 30.95$; *Nfatc4*, $P = 0.4248$ ICD – EGFP, $F = 40.42$). Error bars represent mean ± s.d. Shown graphs are representative of three different independent experiments. $N = 3$ different RNA preparations and analyses.

neurons infected with a lentivirus expressing NRG1 ICD, not infected or infected with a lentivirus expressing EGFP as controls. Of the genes upregulated with a fold change cut-off of 2.0 ($P < 0.01$), *L-pgds* was the most upregulated in DRG neurons overexpressing NRG1 ICD (**Fig. 2**, **Supplementary Fig. 1a,b** and **Supplementary Table 1**).

We next confirmed upregulation of *L-pgds* by RT-PCR (**Supplementary Fig. 1c**) and quantitative RT-PCR (qRT-PCR) analyses (**Fig. 2b**) of mRNA prepared from DRG neurons infected as described above. In addition, we validated these results by determining mRNA levels of *Nfatc4* and *Sod3*, two genes whose expression was above threshold. As expected, we observed that the latter were not exclusively upregulated in NRG1 ICD–infected neurons (**Fig. 2d**). Furthermore, we found that *L-pgds* mRNA expression was increased in mouse DRG neurons only when co-cultured in the presence of rat primary Schwann cells, suggesting that the physiological interaction of Schwann cells with DRG neurons induced *L-pgds* expression (**Fig. 2c**). These results strongly indicate that NRG1 type III intracellular processing induces a specific activation of *L-pgds* mRNA in DRG neurons that is Schwann cell dependent.

L-PGDS is released in the extracellular media

Our results suggest that intracellular processing of NRG1 type III activates the transcription of *L-pgds*, but do not provide any indication as to protein expression or its possible role in PNS. To determine whether L-PGDS protein is also upregulated with its mRNA, we measured L-PGDS protein levels by western blotting and by mass spectrometry shotgun analyses in lysates prepared from NRG1 ICD–infected neurons. To our surprise, we were not able to detect it (**Supplementary Fig. 2a** and data not shown), strongly suggesting that *L-pgds* mRNA is not translated or that the protein is quickly degraded or released into the extracellular media, as previously reported[20,21].

To assess whether L-PGDS protein is released by DRG neurons, we grew both NRG1 ICD–infected and not infected neurons in neurobasal media. We then collected the media after 48 h (**Fig. 3**) and determined L-PGDS expression by western blot. As expected, we detected L-PGDS protein in the conditioned media of neurons infected with NRG1 ICD (**Fig. 3a** and **Supplementary Fig. 2c**) or L-PGDS (**Supplementary Fig. 2b**), but we also detected a very limited amount of L-PGDS in the conditioned media of not infected DRG neurons, indicating that L-PGDS could be constitutively released and that its synthesis is upregulated by NRG1 ICD. We next sought to investigate the functional role of released L-PGDS. Given that L-PGDS is secreted via exosomes[22], we first determined whether Schwann cells could take it up. We grew purified primary rat Schwann cells in the presence of conditioned media prepared from DRG neurons infected with NRG1 ICD and analyzed L-PGDS expression in Schwann cells lysates by western blotting. Unlike the media, which retained L-PGDS expression, we never observed L-PGDS in Schwann cells lysates (**Fig. 3b** and **Supplementary Fig. 2c**).

Given that L-PGDS catalyzes the formation of prostaglandins, we determined whether it is enzymatically active in the extracellular media. Using liquid chromatography tandem mass spectrometry (LC-MS/MS), we measured the amount of PGD2, an L-PGDS metabolite, in conditioned media of DRG neurons that were either not infected or were infected with NRG1 ICD or EGFP. Only the conditioned media of neurons overexpressing NRG1 ICD accumulated PGD2. Notably, the conditioned media of DRG neurons infected with NRG1 ICD and cultured in the presence of AT-56, a specific L-PGDS

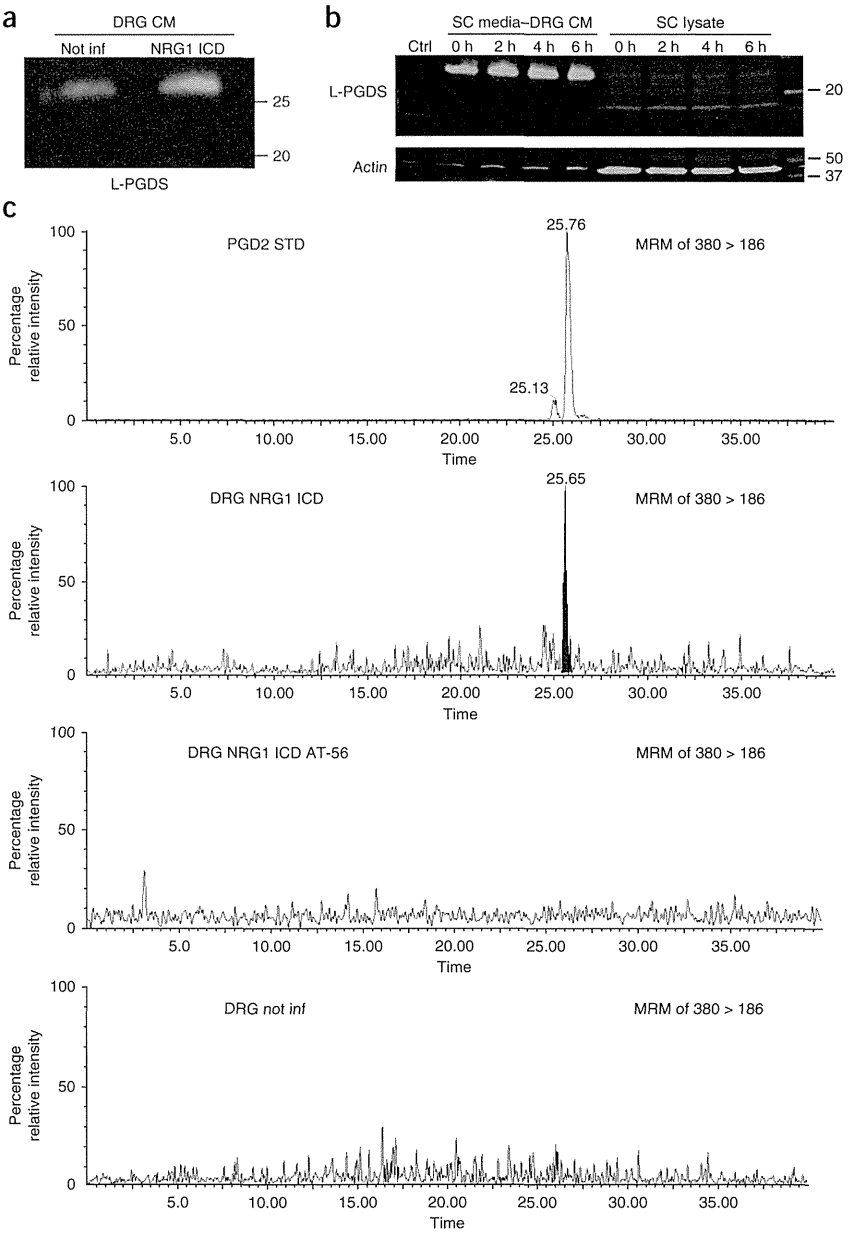

Figure 3 L-PGDS is secreted and enzymatically active. (**a**) Representative western blotting analyses of centrifuged DRG conditioned media (CM) from not infected or NRG1 ICD–infected DRG neurons. Cultures were infected the day after dissection, purified of endogenous Schwann cells (SCs) and grown for additional 14 d to allow lentivirus expression. Neurons were then grown in the presence of neurobasal media for additional 48 h, after which the media was tested for L-PGDS expression. L-PGDS was present in all samples and its levels were increased in NRG1 ICD–infected neurons. $N = 3$ independent experiments. (**b**) Conditioned media of DRG neurons infected with a lentivirus encoding for NRG1 ICD was prepared as in **a**. Primary rat Schwann cells were grown in the presence of collected DRG media for 2, 4 or 6 h, after which Schwann cells were lysed and tested for L-PGDS uptake by western blot. L-PGDS protein was not detected in Schwann cell lysates. Actin served as a control and was mainly present in lysates. The little amount of actin present in DRG conditioned media was probably a result of dead Schwann cells present in the supernatant. Regular Schwann cell growth media was used as a control. The image is representative of three different independent experiments. (**c**) PGD2 was detected by LC-MS/MS in conditioned media of DRG neurons overexpressing NRG1 ICD and in standard solution of PGD2, whereas, in conditioned media of wild-type DRG neurons, PGD2 was undetectable. Note that PGD2 did not accumulate in conditioned media of DRG neurons overexpressing NRG1 ICD treated with AT-56, a specific PGD2 inhibitor. Chromatograms are representative of three different experiments. For uncropped pictures of western blots, see **Supplementary Figure 10**. $N = 3$ conditioned media preparations.

inhibitor[23], did not accumulate PGD2 (**Fig. 3c** and **Supplementary Fig. 2e**). In conclusion, our results indicate that L-PGDS is released into the extracellular media, where maintains its enzymatic activity, as it was able to process PGH2 into PGD2.

L-pgds$^{-/-}$ sciatic nerves are hypomyelinated

PGD2 is the product of two different enzymes, H-PGDS, which is essentially expressed in inflammatory cells and in microglial cells, and L-PGDS, whose expression is enriched in brain[8] and sensory neurons[24]. To confirm the role of L-PGDS in myelination, we analyzed nerve morphology in *L-pgds*$^{-/-}$ mice. These mice display various abnormalities, including glucose intolerance and insulin resistance[25], sleep inhibition[26], acceleration of beta-amyloid deposition[27], and aberrant Sertoli cells maturation[28].

We analyzed sciatic nerves morphology in 1-month-old (**Fig. 4a–c**) and 6-month-old (**Fig. 4d–f**) *L-pgds*$^{-/-}$ mice. At both ages, myelin in *L-pgds*$^{-/-}$ sciatic nerves was noticeably thinner than that of wild-type mice. Morphometric analyses confirmed a significant increase in *g* ratio (axon diameter versus fiber diameter) in *L-pgds*$^{-/-}$ mice versus wild-type littermates (**Supplementary Table 2**) across a range of fibers, whereas axon diameters in adult nerves were comparable in 1-month-old mice and slightly increased in 6-month-old *L-pgds*$^{-/-}$ nerves. We also determined whether a lack of L-PGDS impaired Schwann cells development. We did not find any alteration in the expression of Pou3f1 (Oct6, Scip, Tst1) and Egr2 (Krox-20) or in Schwann cell survival and proliferation in postnatal day 2 (P2) *L-pgds*$^{-/-}$ nerves (**Supplementary Table 3**).

Next, we assessed H-PGDS expression in PNS. Immunohistochemical analyses showed that H-PGDS was expressed in 2-month-old sciatic nerves and it was not upregulated in *L-pgds*$^{-/-}$ nerves (**Supplementary Fig. 3a**). Furthermore, morphological analyses of 1-month-old and 6-month-old *H-pgds*$^{-/-}$ sciatic nerves revealed that, at both ages, *H-pgds*$^{-/-}$ sciatic nerves were normally myelinated (**Supplementary Table 2** and **Supplementary Fig. 3b–g**).

H-pgds$^{-/-}$; *L-pgds*$^{-/-}$ mice are hypomyelinated and myelin is aberrant

To determine whether a lack of both *H-pgds* and *L-pgds* would worsen the hypomyelinating phenotype, we analyzed *in vitro* and *in vivo* myelination in the absence of both enzymes. We first analyzed

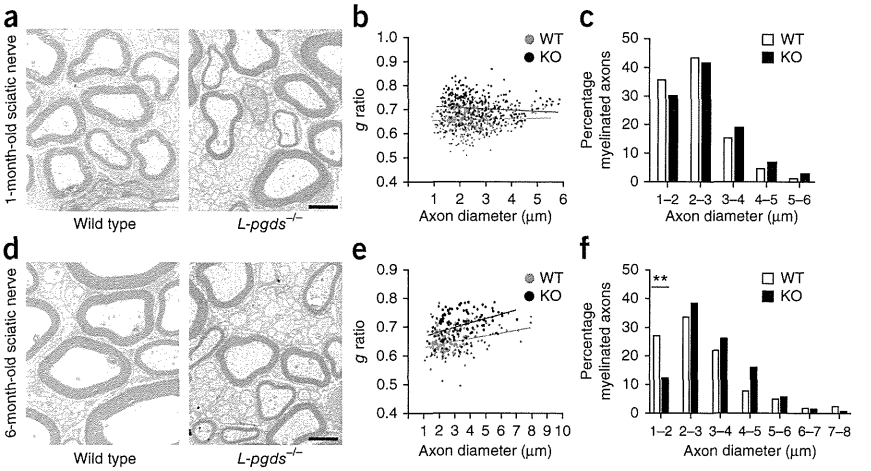

Figure 4 *L-pgds*$^{-/-}$ are hypomyelinated. (**a–c**) Morphological analyses of 1-month-old wild-type (WT) and *L-pgds*$^{-/-}$ (KO) sciatic nerves. Electron micrographs (**a**) and *g* ratio analyses (**b**) confirmed hypomyelination in *L-pgds*$^{-/-}$ nerves. *g* ratio was significantly different between wild-type (red line) and *L-pgds*$^{-/-}$ 1-month-old mice (black line; *t* test analysis, $P \leq 0.0001$, $t = 13.19$, df = 782). The graph represents the *g* ratio obtained from more than 300 myelinated axons. (**c**) Distribution of myelinated fibers is similar in *L-pgds*$^{-/-}$ and wild-type 1-month-old sciatic nerves (Fisher's exact test; $P = 0.2811$ (total versus 1–2 μm), $P = 0.7437$ (total versus 2–3 μm), $P = 0.2618$ (total versus 3–4 μm), $P = 0.2776$ (total versus 4–5 μm), $P = 0.1917$ (total versus 5–6 μm)). Over 100 fibers for each genotype were counted. Scale bar represents 2 μm. (**d–f**) Morphological analyses of 6-month-old wild-type and *L-pgds*$^{-/-}$ sciatic nerves. Electron micrographs (**d**) and *g* ratio analyses (**e**) confirmed hypomyelination in *L-pgds*$^{-/-}$ nerves. *g* ratio was significantly different between wild-type (red line) and *L-pgds*$^{-/-}$ 6-month-old mice (black line; *t* test analysis, $P \leq 0.0001$, $t = 9.983$, df = 292). The graph represents the *g* ratio obtained from more than 150 myelinated axons. (**f**) Distribution of myelinated fibers is similar in *L-pgds*$^{-/-}$ and wild-type 6-month-old sciatic nerves, with a significant slight decrease in small fibers (1–2 um) in *L-pgds*$^{-/-}$ nerves (Fisher's exact test; $^{**}P = 0.0097$ (total versus 1–2 μm), $P = 0.6492$ (total versus 2–3 μm), $P = 0.595$ (total versus 3–4 μm), $P = 0.0694$ (total versus 4–5 μm), $P = 1$ (total versus 5–6 μm), $P = 1$ (total versus 6–7 μm), $P = 0.3759$ (total versus 7–8 μm)). Over 60 fibers for each genotype were counted. Scale bar represents 2 μm. $N = 3$ mice per genotype at each time developmental time point.

ultrastructural myelin *in vitro* in myelinating co-cultures. We prepared DRG neurons from *H-pgds*$^{-/-}$; *L-pgds*$^{-/-}$ mice at embryonic day 14.5 (E14.5), purified of endogenous Schwann cells and fibroblasts by antimitotic treatment and seeded with wild-type rat Schwann cells. Myelination was induced by adding 50 μg ml^{-1} ascorbic acid for 9 d, after which cultures were processed for immunofluorescence (data not shown) and electron microscopy analyses (**Supplementary Fig. 4**). The number of naked axons was increased in null co-cultures. Notably, *H-pgds*$^{-/-}$; *L-pgds*$^{-/-}$ DRG neurons were substantially hypomyelinated, unlike wild-type controls (**Supplementary Fig. 4c**). Furthermore, we found that, when formed, myelin in *H-pgds*$^{-/-}$; *L-pgds*$^{-/-}$ cultures was aberrant.

Next, we analyzed sciatic nerve morphology in newborn and adult *H-pgds*$^{-/-}$; *L-pgds*$^{-/-}$. We did not observe axonal sorting defects 2 d after birth in *H-pgds*$^{-/-}$; *L-pgds*$^{-/-}$ as compared with controls, although *H-pgds*$^{-/-}$; *L-pgds*$^{-/-}$ fibers were hypomyelinated (**Supplementary Fig. 5a**). We then determined sciatic nerve morphology by electron microscopy analyses and *g* ratio measurements in 7-d-old (**Fig. 5a–c**), 1-month-old (**Fig. 5d–f**) and 9-month-old *H-pgds*$^{-/-}$; *L-pgds*$^{-/-}$ mice (**Fig. 5g–i**). At all ages, *H-pgds*$^{-/-}$; *L-pgds*$^{-/-}$ sciatic nerves fibers were hypomyelinated when compared with those of comparable size in wild-type mice. Morphometric analyses confirmed increased *g* ratio in *H-pgds*$^{-/-}$; *L-pgds*$^{-/-}$ mice versus wild-type littermates (**Supplementary Table 2**), whereas axon diameters in adult nerves were comparable. In addition, in aged *H-pgds*$^{-/-}$; *L-pgds*$^{-/-}$ sciatic nerves, myelin was aberrant (**Fig. 5j,k**), resembling the phenotype observed *in vitro*. We found similar alterations in 6-month-old sciatic nerves of *L-pgds*$^{-/-}$ mice, although the difference was not significant ($P = 0.0649$; **Supplementary Table 2**). Notably, we did not find such alterations in 1-month-old *H-pgds*$^{-/-}$; *L-pgds*$^{-/-}$ nerves, suggesting that these defects are possibly the result of demyelinating events.

To determine whether the hypomyelinating phenotype is more pronounced in sensory nerves, we analyzed myelination in 8-month-old *H-pgds*$^{-/-}$; *L-pgds*$^{-/-}$ saphenous nerves (**Supplementary Fig. 5b–d** and **Supplementary Table 2**). We found that *H-pgds*$^{-/-}$; *L-pgds*$^{-/-}$ nerves were hypomyelinated as compared with wild-type controls. Notably, the total number of myelinated fibers was similar in wild-type and *H-pgds*$^{-/-}$; *L-pgds*$^{-/-}$ motor and sensory roots (**Supplementary Fig. 6a–d**) and distally in sciatic nerves (**Supplementary Fig. 6e**), indicating that *L-pgds* has no effects on neuronal cell number. Similarly, the distribution of axons per Remak bundle was comparable in wild-type and *H-pgds*$^{-/-}$; *L-pgds*$^{-/-}$ nerves at both 1 and 9 months of age (**Supplementary Fig. 6f,g**). Collectively, these findings indicate that L-PGDS is relevant for myelin formation, whereas H-PGDS is dispensable. Furthermore, they suggest that NRG1 backward signaling and PGD2 production are most likely involved in myelin maintenance.

L-PGDS enzymatic activity is important for PNS myelination

Our results suggest that released L-PGDS is enzymatically active. To better investigate its mechanism of action, we inhibited L-PGDS in a Schwann cell–neuronal myelinating co-culture system. We used the specific competitive L-PGDS inhibitor AT-56. To obtain optimal inhibition and avoid toxic effects, we first titrated the amount of AT-56 and compared it with vehicle (DMSO)-treated cultures. We treated isolated rat primary Schwann cells and purified mouse DRG neurons with various AT-56 concentrations for 13 d and monitored cell death by active caspase 3 staining. We found that 50 μM AT-56 induced significant cell death in both neurons (data not shown) and Schwann cells ($P < 0.0001$; **Supplementary Fig. 7a**), whereas 20 and 30 μM AT-56 were well tolerated and did not induce any cell sufferance or death. We analyzed whether 7 d of treatment with 25 and 50 μM AT-56 affected survival in non-myelinating Schwann cell–DRG neuronal co-cultures. We could not detect any caspase 3 activation (**Supplementary Fig. 7c**). Similarly, we did not observe any effect of AT-56 on axon–Schwann cell association (**Supplementary Fig. 7d**).

Next, we induced myelination in organotypic Schwann cell–DRG neuronal co-cultures by adding 50 μg ml^{-1} of ascorbic acid in the presence or absence of AT-56. We added 25 μM AT-56 to the culture media every other day, starting the day before addition of ascorbic acid and continued for 7 or 21 d (**Fig. 6a–d**). Immunofluorescence (**Fig. 6a**)

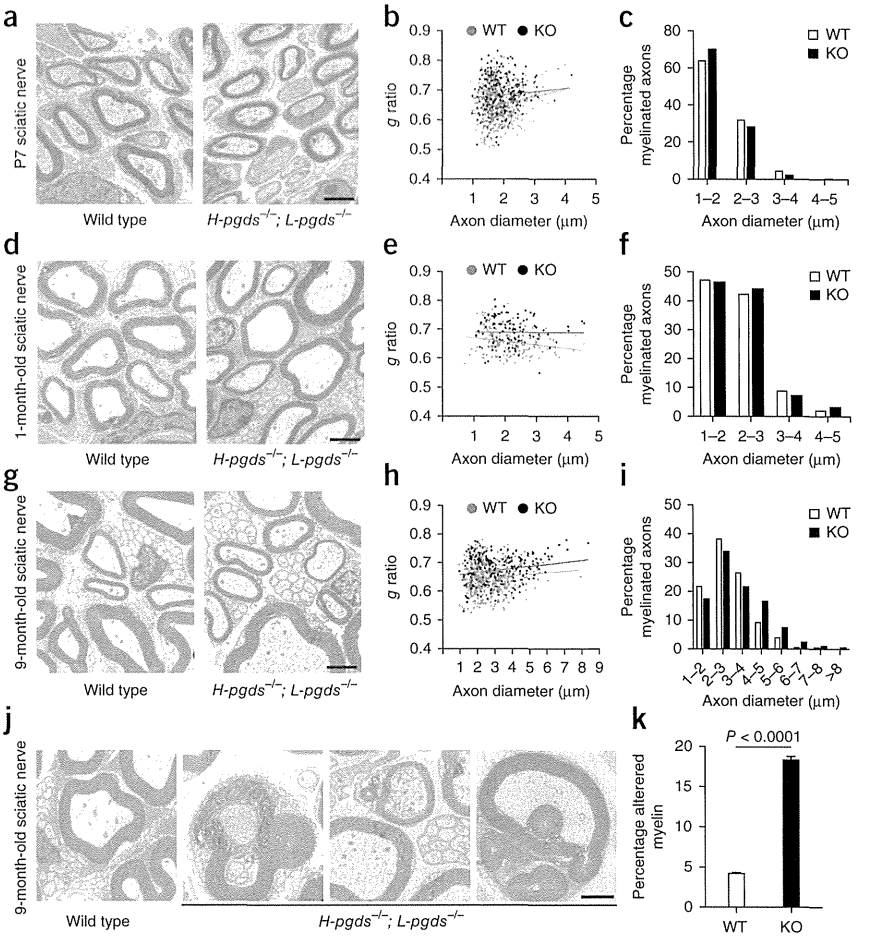

Figure 5 *H-pgds* and *L-pgds* are required for myelin formation and maintenance. (**a–c**) Morphological analyses of P7 wild-type and *H-pgds*$^{-/-}$; *L-pgds*$^{-/-}$ sciatic nerves. Electron micrographs (**a**) and *g* ratio analyses (**b**) confirmed hypomyelination in *H-pgds*$^{-/-}$; *L-pgds*$^{-/-}$ nerves. *g* ratio was significantly different between wild-type (red line) and P7 *H-pgds*$^{-/-}$; *L-PGDS*$^{-/-}$ (black line; *t* test analysis, $P \leq 0.0001$, $t = 6.308$, df = 713). The graph represents the *g* ratio obtained from more than 300 myelinated axons. (**c**) Distribution of myelinated fibers was similar in *H-pgds*$^{-/-}$; *L-pgds*$^{-/-}$ and wild-type P7 sciatic nerves (Fisher's exact test; $P = 0.4774$ (total versus 1–2 μm), $P = 0.5307$ (total versus 2–3 μm), $P = 0.0808$ (total versus 3–4 μm), $P = 1$ (total versus 4–5 μm)). Over 100 fibers for each genotype were counted. $N = 3$ mice per genotype. Scale bar represents 2 μm. (**d–f**) Morphological analyses of 1-month-old wild-type and *H-pgds*$^{-/-}$; *L-pgds*$^{-/-}$ sciatic nerves. Electron micrographs (**d**) and *g* ratio analyses (**e**) confirmed hypomyelination in *H-pgds*$^{-/-}$; *L-pgds*$^{-/-}$ nerves. *g* ratio was significantly different between wild-type (red line) and *H-pgds*$^{-/-}$; *L-pgds*$^{-/-}$ (black line; *t* test analysis, $P \leq 0.0001$, $t = 6.104$, df = 272). The graph represents the *g* ratio obtained from more than 120 myelinated axons. (**f**) Distribution of myelinated fibers is similar in *H-pgds*$^{-/-}$; *L-pgds*$^{-/-}$ and wild-type 1-month-old sciatic nerves (Fisher's exact test; $P = 0.9143$ (total versus 1–2 μm), $P = 0.9124$ (total versus 2–3 μm), $P = 0.8245$ (total versus 3–4 μm), $P = 0.7071$ (total versus 4–5 μm)). Over 40 fibers for each genotype were counted. $N = 3$ mice per genotype. Scale bar represents 2 μm. (**g–i**) Morphological analyses of 9-month-old wild-type and *H-pgds*$^{-/-}$; *L-pgds*$^{-/-}$ sciatic nerves. Electron micrographs (**g**) and *g* ratio analyses (**h**) confirmed hypomyelination in *H-pgds*$^{-/-}$; *L-pgds*$^{-/-}$ nerves. *g* ratio was significantly different between wild-type (red line) and *H-pgds*$^{-/-}$; *L-pgds*$^{-/-}$ (black line; *t* test analysis, $P \leq 0.0001$, $t = 6.386$, df = 694). The graph represents the *g* ratio obtained from more than 300 myelinated axons. (**i**) Distribution of myelinated fibers is similar in *H-pgds*$^{-/-}$; *L-pgds*$^{-/-}$ and wild-type 9-month-old sciatic nerves (Fisher's exact test; $P = 0.6116$ (total versus 1–2 μm), $P = 0.5183$ (total versus 2–3 μm), $P = 0.5299$ (total versus 3–4 μm), $P = 0.0754$ (total versus 4–5 μm), $P = 0.162$ (total versus 5–6 μm), $P = 0.2168$ (total versus 6–7 μm), $P = 1$ (total versus 7–8 μm), $P = 1$ (total versus >8 μm)). Over 100 fibers for each genotype were counted. $N = 3$ mice per genotype. Scale bar represents 2 μm. (**j**) Electron microscopy images of 9-month-old myelinated fibers in wild-type and *H-pgds*$^{-/-}$; *L-pgds*$^{-/-}$ sciatic nerves. Myelin was aberrant in *H-pgds*$^{-/-}$; *L-pgds*$^{-/-}$, but not in wild-type, fibers. $N = 3$ mice per genotype. Scale bar represents 2 μm. (**k**) Graph representing the percentage of axons with altered myelination in *H-pgds*$^{-/-}$; *L-pgds*$^{-/-}$ versus wild-type 9-month-old mice. All counting was performed on reconstructed sciatic nerve and the results expressed relative to the total number of myelinated fibers. Over 1,000 fibers for each genotype were counted (*t* test analysis, $P \leq 0.0001$, $t = 24.17$, df = 4). $N = 3$ mice per genotype. Error bars represent mean ± s.e.m.

and western blot analyses (**Fig. 6b**) revealed that AT-56 addition substantially inhibited myelin basic protein (MBP) and myelin protein zero (MPZ) expression as compared with untreated or DMSO-treated cultures with a dose-dependent effect (**Supplementary Fig. 7b**), but had no effect on internodal length (**Fig. 6d**). We further confirmed these results by assessing the numbers of MBP$^+$ segments, which were significantly diminished in AT-56 treated as compared with untreated or DMSO-treated co-cultures ($P < 0.0001$; **Fig. 6c**). These data confirm that L-PGDS enzymatic activity is important in myelin formation, although we cannot exclude the possibility that AT-56 might affect Schwann cells survival and/or axon association in myelinating conditions.

Our *in vivo* analyses suggest that PGD2 might be important for myelin maintenance. Thus, we inhibited L-PGDS signaling *in vitro* in already myelinated cultures. We added 25 μM AT56 to wild-type Schwann cell neuronal co-cultures that had already been myelinated for 21 d. Cultures were maintained for an additional 7 d and the inhibitor was added every other day (concomitantly with the change of media). AT-56 treatment resulted in marked demyelination (**Fig. 6e**), as corroborated also electron microscopy analyses (**Fig. 6f**). These results confirm that NRG1 backward signaling and PGD2 production might be involved in myelin maintenance.

Gpr44 regulates PNS myelination

PGD2 can bind to two G protein–coupled transmembrane receptors: *Gpr44* (also known as *Ptgdr2* or *Crth2*) and *Ptgdr* (also known as *DP*). To determine which receptor is the target of PGD2, we investigated mRNA expression levels of both receptors by quantitative PCR (qPCR) in DRG neurons that were either infected or not with NRG1 ICD and in purified primary rat Schwann cells. Although *Ptgdr* expression level was similar in all samples (**Supplementary Fig. 8a**), *Gpr44* was highly expressed in purified primary rat Schwann cells as compared

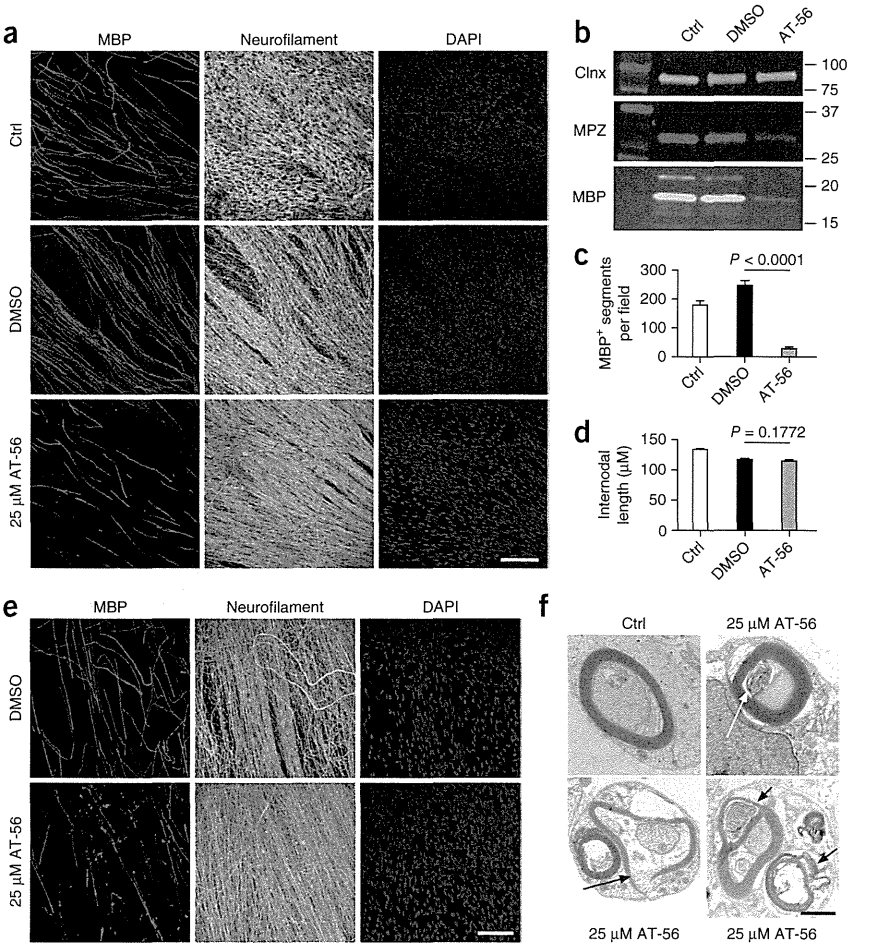

Figure 6 L-PGDS enzymatic activity is important for PNS myelination and maintenance. (**a**) Representative immunofluorescence of co-cultures of organotypic rat Schwann cells and DRG neurons treated with 25 μM AT-56 for 7 d in the presence of ascorbic acid to induce myelination. AT-56 treatment was started the day before ascorbic acid addition and the compound was added every other day. After 7 d in myelinating conditions, cultures were fixed and stained for MBP (rhodamine), neurofilament (fluorescein) and nuclei (DAPI, blue). AT-56 treatment substantially impaired myelination. $N = 5$ different independent co-culture experiments. Scale bar represents 100 μm. (**b**) Representative western blotting analyses of organotypic rat Schwann cell–DRG neuronal co-cultures treated with 25 μM AT-56 for 21 d in myelinating conditions. Lysates were tested for MPZ, MBP and calnexin (Clnx) as a loading control. MBP and MPZ expression were substantially reduced in the presence of AT-56. For uncropped pictures of western blots, see **Supplementary Figure 10**. $N = 5$ different independent experiments. (**c**) Average of three different experiments showing quantitation of MBP$^+$ segments 7 d after induction of myelination in control and 25 μM AT-56–treated co-cultures. Quantitation was performed on the entire culture (t test analyses, $P \leq 0.0001$, $t = 13.66$, df = 76 DMSO – AT-56). Error bars represent mean ± s.e.m. $N = 39$ cultures per condition from three different independent experiments. (**d**) Representative graph showing internodal length of 216 MBP$^+$ segments per condition 21 d after induction of myelination in control and 25 μM AT-56–treated co-cultures. The distance between Nodes of Ranvier was determined by co-staining myelinated cultures with the paranodal marker Caspr. AT-56 treatment had no effect on internodal length (t test analyses, $P = 0.1772$, AT-56–DMSO $t = 1.352$, df = 430). Error bars represent mean ± s.e.m. $N = 216$ segments per condition from three different independent experiments. (**e**) Representative immunofluorescence of already myelinated organotypic rat Schwann cell–DRG neuronal co-cultures (21 d of ascorbic acid) were treated with 25 μM AT-56 for an additional 7 d in myelinating conditions. At the end of the treatment, cultures were fixed and stained for MBP (rhodamine), neurofilament (fluorescein) and nuclei (DAPI, blue). AT-56 treatment in already myelinated cultures induced myelin degeneration. $N = 3$ different independent co-culture experiments. Scale bar represents 100 μm. (**f**) Representative electron microscopy analyses of untreated or 25 μM AT-56–treated Schwann cell–DRG neuronal co-cultures. As in **e**, cultures were allowed to myelinate for 21 d, then treated with 25 μM AT-56 or DMSO as control for additional 7 d. Signs of myelin damage (arrows) were observed only in AT-56–treated cultures resembling those observed *in vivo*. $N = 9$ different independent co-culture experiments. Scale bar represents 1 μm.

with DRG neurons, either infected or not (**Fig. 7a**), suggesting that Gpr44 might function as a glial receptor for PGD2.

Thus, we inactivated *Gpr44* expression using shRNA lentiviral-mediated knockdown *in vitro*. We used three different shRNA clones (shA3, shA5 and shC9) obtained from the siRNA Consortium together with a lentiviral vector expressing a scrambled artificial sequence as a negative control[4]. BLAST analyses confirmed that the targeted sequences, although originally designed in mouse, also recognized rat *Gpr44*. We corroborated efficient knockdown in infected rat primary Schwann cells by qPCR analyses. Two of three *Gpr44* shRNA significantly ablated the expression of *Gpr44* (50–70% reduction; shA3, $P \leq 0.001$; shC9, $P \leq 0.0001$; **Fig. 7b**) when compared with that of not infected or scramble-infected cultures.

We then infected mouse DRG explant cultures containing both Schwann cells and neurons with *Gpr44* shRNA or scramble shRNA as described previously[4]. Cultures were grown without antimitotic agents to allow infection of both neurons and Schwann cells. Myelination was induced by supplementing the cultures with 50 μg ml^{-1} ascorbic acid for 7 d, after which they were analyzed by immunohistochemistry for MBP and neurofilament expression (**Supplementary Fig. 8b**). Notably, downregulation of Gpr44 impaired the extent of myelination *in vitro* in organotypic myelinating co-cultures.

To determine the cell autonomous role of Gpr44, we knocked down its expression in isolated primary rat Schwann cells and co-cultured them with purified mouse wild-type neurons. Efficient knocked down was determined on isolated Schwann cells by qRT-PCR analyses before seeding onto neurons using primers specific for *Gpr44* (**Fig. 7b**). Cultures were maintained in myelinating conditions for 21 d. Immunofluorescence (**Fig. 7c**) and western blotting (**Fig. 7d**) analyses for MBP and neurofilament revealed that ablation of glial Gpr44 substantially impaired myelination, suggesting that *Gpr44* acts Schwann cell autonomously *in vitro*.

To further validate Gpr44's role in PNS myelination, we analyzed *in vivo* myelination in 2-month-old *Gpr44*$^{-/-}$ sciatic nerves. Electron microscopy analyses showed that these nerves were hypomyelinated (**Fig. 7e**). Morphometric analyses confirmed an increased g ratio in

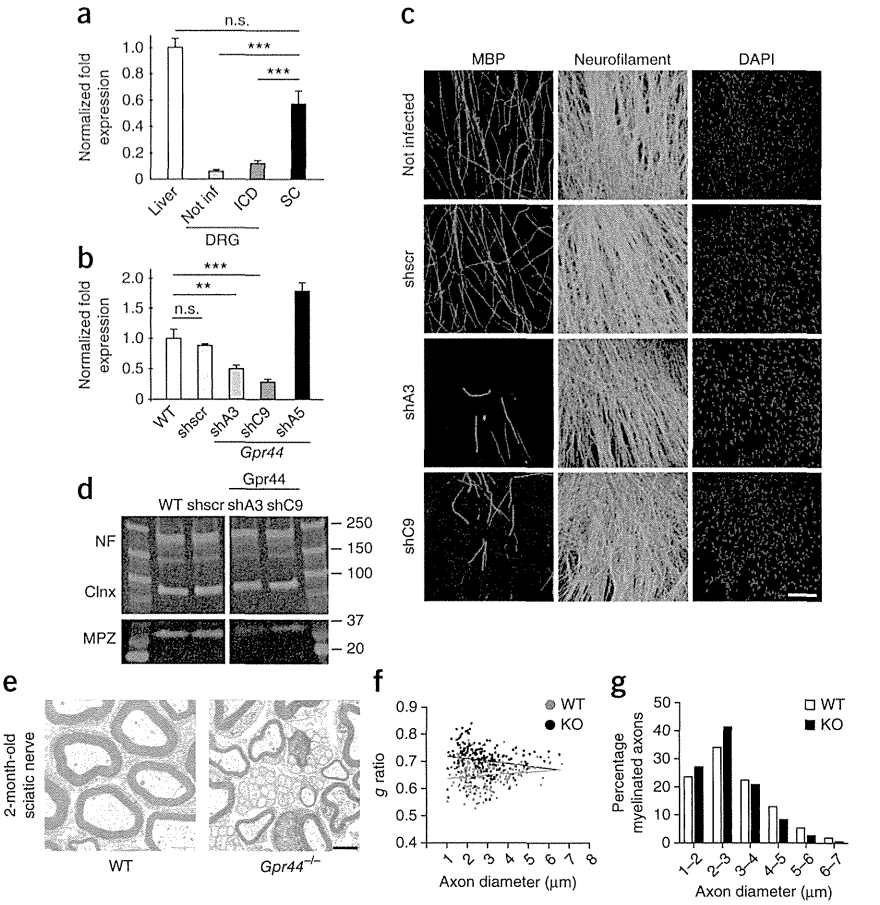

Figure 7 Gpr44 promotes myelination. (**a**) *Gpr44* qRT-PCR analyses in mRNA prepared from not infected or NRG1 ICD–infected DRG neurons, primary rat Schwann cells and liver, which serves as a control. *Gpr44* was significantly expressed in primary rat Schwann cells. Expression levels were normalized to *Gapdh* levels. Data were analyzed with the CFX Manager Software on three mRNA different preparations. Error bars represent mean ± s.d. (one-way ANOVA, $F = 114$, $^{***}P \leq 0.0001$ SC – not inf, $^{***}P \leq 0.0001$ SC – ICD, $P = 0.1755$ SC – liver). $N = 3$ different independent mRNA preparations and analyses. n.s. indicates not significant ($P = 0.1755$). (**b**) Average of three different experiments showing approximately 70% reduction in *Gpr44* expression in Schwann cells infected with *Gpr44* shRNAs (shA3, shC9). Expression levels were determined by qRT-PCR analyses in mRNA prepared from *Gpr44* shRNA–infected, not infected or scramble-infected Schwann cells, which serve as control, and normalized to *Gapdh* levels. Data were analyzed with the CFX Manager Software on three mRNA different preparations. Error bars represent means ± s.e.m. (one-way ANOVA, $F = 98.33$, $^{**}P \leq 0.001$ wild type – shA3, $^{***}P \leq 0.0001$ wild-type – shC9, $P = 0.6408$ wild type – shscr). $N = 3$ different independent infections performed with three different vital stock preparations. (**c**) Representative immunofluorescence of co-cultures of uninfected wild-type mouse DRG neurons purified of endogenous Schwann cells and repopulated with rat Schwann cells previously infected with *Gpr44* shRNA (shA3 or shC9) or scrambled shRNA (shscr). Cultures were maintained in myelinating conditions for 21 d, then stained for MBP (rhodamine) and neurofilament (fluorescein). Fewer myelin segments were evident in shA3- and shC9-treated cultures. $N = 3$ different independent co-culture experiments. Scale bar represents 100 μm. (**d**) Representative western blotting analyses of wild-type uninfected mouse DRG neurons purified of endogenous Schwann cells and repopulated with rat Schwann cells previously infected with shA3, shC9 or shscr. Lysates were tested for MPZ, neurofilament (NF) and calnexin as a loading control, 14 d after induction of myelination. MPZ expression was substantially reduced in *Gpr44* knocked down cultures. For uncropped pictures of western blots, see **Supplementary Figure 10**. $N = 3$ different independent experiments. (**e–g**) Morphological analyses of 2-month-old wild-type and $Gpr44^{-/-}$ sciatic nerves. Electron micrographs (**e**) and *g* ratio analyses (**f**) confirmed hypomyelination in $Gpr44^{-/-}$ nerves. *g* ratio was significantly different between wild-type (red line) and $Gpr44^{-/-}$ (black line) nerves (*t* test analysis, $P \leq 0.0001$, $t = 8.048$, df = 391). The graph represent the *g* ratio obtained from more than 150 myelinated axons. (**g**) Distribution of myelinated fibers was similar in $Gpr44^{-/-}$ and wild-type 2-month-old sciatic nerves (Fisher's exact test; $P = 0.5733$ (total versus 1–2 μm), $P = 0.3816$ (total versus 2–3 μm), $P = 0.8086$ (total versus 3–4 μm), $P = 0.182$ (total versus 4–5 μm), $P = 0.2889$ (total versus 5–6 μm), $P = 0.3219$ (total versus 6–7 μm)). Over 70 fibers for each genotype were counted. $N = 3$ mice per genotype. Over 60 fibers for each genotype were counted. Scale bar represents 2 μm.

$Gpr44^{-/-}$ mice versus wild-type littermates (**Supplementary Table 2**), mainly in small fibers, whereas axon diameters in adult nerves were comparable (**Fig. 7f,g**). Collectively, these results indicate that Gpr44 participates in PNS myelination, although we could not prove that it is directly activated by L-PGDS, as the addition of 15R-methyl-prostaglandin D2, a specific Gpr44 agonist, had a toxic effect onto $H\text{-}pgds^{-/-}; L\text{-}pgds^{-/-}$ *in vitro* co-cultures (data not shown).

PGD2 activates Nfatc4 in Schwann cells

We sought to determine the signaling pathways activated by PGD2 in Schwann cells. Previous studies in immune cells reported that Gpr44 activation can mobilize intracellular Ca^{2+} storage or modulate intracellular levels of cAMP[16]. Notably, in PNS myelination, PLC-γ, via the NRG1/erbB pathway, increases intracellular Ca^{2+} levels and promotes nuclear translocation of the transcription factor Nfat-c3/c4 in Schwann cells to induce myelination[18]. Furthermore, elevation of cAMP in rat primary Schwann cells activates transcription of myelin genes[29,30]. In addition to these pathways, NRG1 type III specifically activates the PI-3 kinase pathway[31,32], and recent studies have shown that ablation of the ERK/MAPK pathways prevents PNS myelination[33].

Thus, we investigated which signaling pathways, among those implicated in myelination, are activated by PGD2. Primary rat Schwann cells were grown to confluence, starved for 16 h, stimulated with 100 nM PGD2 for 30 min at 37 °C, lysed and the extracts were run on a SDS gel for western blot analyses. PKA phosphorylation was not altered following PGD2 stimulation, suggesting that PGD2 does not modulate cAMP activity (**Fig. 8a**). Notably, although phospho-AKT, MAPK (**Supplementary Fig. 9a,b**) and calcineurin B1 (**Fig. 8b**) levels were not differentially regulated, PGD2 caused a shift in Nfatc4 phosphorylation (**Fig. 8c**)[18] without altering its total levels. Next, we determined whether Gpr44 knockdown in Schwann cells would alter Nfatc4 phosphorylation. Western blotting analyses did not reveal any effect, indicating either that Nfatc4 could also be modulated by other

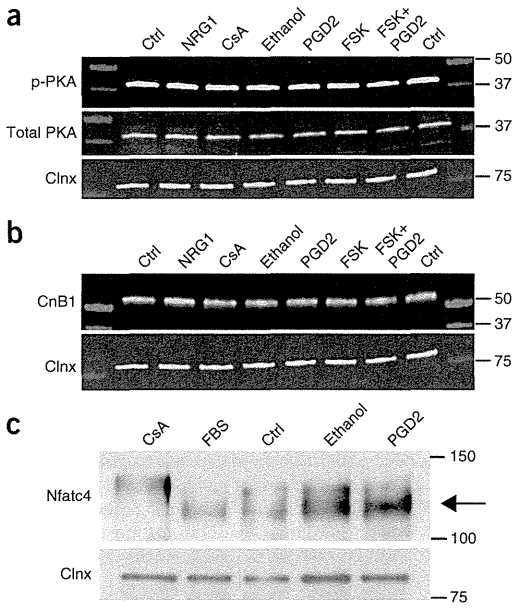

Figure 8 PGD2 induced Nfatc4 dephosphorylation in primary Schwann cells. Rat primary Schwann cells were grown to confluence and then starved for 16 h. Schwann cells were treated with 2.5 ng ml^{-1} NRG1β1, 10 nM cyclosporin A, 100 nM ethanol, 100 nM PGD2, 2.5 μM forskolin, 100 nM PGD2 and 2.5 μM forskolin. (**a**,**b**) Schwann cells lysates were tested by western blotting analyses for phosphorylated and total PKA levels (**a**) and for calcineurin B1 (**b**), whose expression levels did not change. Images are representative of different experiments. For uncropped pictures of western blots, see **Supplementary Figure 10**. $N = 3$ independent experiments. (**c**) Starved Schwann cells as in **a** were stimulated with 10 nM cyclosporin A, 100 nM ethanol and 100 nM PGD2. In all experiments, not starved (FBS) and starved but not stimulated Schwann cells were also tested (Ctrl). Schwann cells lysates were assayed by western blotting analyses for total Nfatc4 levels. PGD2 induced dephosphorylation of Nfatc4 (arrow). Image is representative of different experiments. $N = 5$ independent experiments.

receptors or that the knockdown we obtained in primary Schwann cells (50–70%) might not be sufficient (data not shown). Collectively, these results indicate that NRG1 backward signaling specifically activates L-PGDS neuronal release and most likely activates Gpr44 on Schwann cells, identifying a previously unknown pathway in PNS myelination (**Supplementary Fig. 9c**).

DISCUSSION

Regulated intramembrane proteolysis is a highly conserved mechanism, allowing fast communication from the plasma membrane to the cell nucleus, where the response to extracellular stimuli is normally achieved by activating the transcription of specific genes[34]. Our data indicate that, in the PNS, NRG1 type III, similar to other growth factors, is processed following a regulated intramembrane proteolysis mechanism. Furthermore, our data describe a previously unknown, pharmacologically accessible level of communication between Schwann cells and neurons. We found that Schwann cells are important regulators of NRG1 processing together with the γ-secretase complex. Although our preliminary data show that erbB receptors are not sufficient to mediate NRG1 cleavage (data not shown), it is possible that they act in synergy with other molecules.

Our main result is the identification of L-PGDS and of the G protein–coupled receptor Gpr44, which has almost exclusively been implicated in inflammatory processes[35], as key determinants in PNS myelin formation and maintenance. Collectively, our data suggest that this class of molecules is not simply a key mediator of cell-cell interaction in dendritic cells[36], but exerts this role in other biological systems, including PNS.

We found that, following NRG1 intracellular domain cleavage and nuclear translocation, *L-pgds* mRNA was upregulated inside the neurons, whereas L-PGDS protein was secreted. Although L-PGDS secretion has been reported in other systems[11,20,27,37], how this is achieved in PNS is currently unknown. Previous studies have shown that L-PGDS is released together with PGD2 via exosomes. In addition to L-PGDS and PGD2, exosomes contain all of the enzymes and substrates necessary for prostaglandin production, including arachidonic acid, Cox-1 (Ptgs1), Cox-2 (Ptgs2) and PGH2, suggesting that these vesicles can behave as carriers of bioactive lipids[22]. Whether *L-pgds* mRNA is transported along neurites and then locally translated before insertion in exosomes has not yet been determined. Alternatively, L-PGDS protein, similar to BDNF, could be internally synthesized and immediately processed by fast transport turnover[38]. As in the case of BDNF in fact, L-PGDS endogenous neuronal levels are extremely limited, thus L-PGDS protein might be translated in neurons and then trafficked trough the secretory pathway by chaperone proteins[39].

Previous studies have implicated the NRG1 intracellular domain in the promotion of neuronal survival[5]. Unlike these results, we could not confirm that NRG1 ICD has a similar role *in vitro* in DRG neurons and we could not find alterations in the number of myelinated fibers *in vivo*. Our study differs from the previous one[5] in that we investigated NRG1 ICD in PNS neurons, whereas the previous study used hippocampal neurons, suggesting that the effects of NRG1 ICD could vary in different neuronal populations. It is also possible, however, that *in vitro* analyses of neuronal survival mediated by these prostanoids might be masked[40].

Notably, NRG1 ICD specifically and substantially upregulated the expression of *L-pgds*, which is enzymatically active to produce the bioactive prostaglandin PGD2. We found that PGD2 most likely activated Gpr44 on Schwann cells to promote myelin formation. Stimulation of Gpr44 ultimately led to dephosphorylation of the transcription factor Nfatc4, a triggering event for the expression of *Egr2* and *MPZ*[18]. Consistent with a previous study[18], we also found that activation of Nfatc4 was independent of the PI-3 kinase and MAPK pathways, but was specifically modulated by PGD2. Unlike previous studies, activation of Nfatc4 downstream of PGD2 did not require increased levels of intracellular cAMP[41], although cAMP might cooperate with PGD2 to activate Nfat in Schwann cells.

In our analyses, we also characterized a G protein–coupled receptor, Gpr44, that participated in PNS myelination. The role of G protein–coupled receptors in myelination has been studied previously. Although many have been implicated in the control and modulation of CNS myelination and remyelination[42,43], the only member of this family thus far implicated in PNS myelination is adhesion G protein–coupled receptor 126 (Gpr126), in both zebrafish[44] and mammals[45]. Gpr126 activity, unlike Gpr44, is dependent on PKA phosphorylation[46,47] and increased intracellular levels of cAMP[47]. Recent studies have shown that, at least in zebrafish, the pathways activated by NRG1 type III and Gpr126 are both required for initiation of myelination *in vivo*, but that different signals control initiation and maturation of myelin[46]. Our results suggest that Gpr44 could be part of the signaling machinery that, in synergy with NRG1 type III, could be involved in myelin maintenance. Nonetheless, we cannot exclude the possibility that other PGD2 receptors, particularly Ptgdr, which is expressed by both Schwann cells and neurons, might participate.

Our *in vitro* and *in vivo* analyses indicate that L-PGDS contributes to myelin formation. However, the *in vivo* phenotype was not as severe as the one observed *in vitro*. Whether this is the result of an exacerbation of *in vitro* settings or of compensation from other prostaglandins expressed in the nerves is remains unknown. Our study excludes the possibility that H-PGDS contributes to the phenotype, although it has been reported that other members of the lipocalin family, such as ApoD and ApoE, are important during regeneration following nerve injury[48,49]. Furthermore, it is possible that L-PGDS and Gpr44 act preferentially onto sensory fibers, as suggested by the marked hypomyelination of small fibers in *Gpr44*$^{-/-}$ and increased *g* ratio values in saphenous nerves.

The hypomyelinating phenotype is similar in *L-pgds*$^{-/-}$ and *H-pgds*$^{-/-}$; *L-pgds*$^{-/-}$ mice. However, only in aged *H-pgds*$^{-/-}$; *L-pgds*$^{-/-}$ mice was myelin significantly altered ($P < 0.0001$), suggesting that PGD2 might be important for myelin stability, as supported by *in vitro* studies. Although we observed some fibers with aberrant myelin in 6-month-old *L-pgds*$^{-/-}$ mice, the precise mechanism implicating PGD2 in myelin formation and maintenance remains unclear. Whether L-PGDS and Gpr44 simply stabilize the adhesion at the adaxonal membrane or represent an extra checkpoint for myelination is unknown. Initiation of myelination and the amount of myelin formed depends on NRG1 type III forward signaling, although it is possible that L-PGDS, activated by NRG1 itself, signals back to Schwann cells to stabilize myelin. In the absence of L-PGDS, this checkpoint is lacking and the myelin formed is unstable, resulting in fast and continuous remodeling. Alternatively, L-PGDS and Gpr44 could be part of a feedback mechanism by which the axon is communicating to Schwann cells its integrity, indicating that myelination can continue. We favor the latter hypothesis, as hypomyelination in older animals was accompanied by severe myelin alterations, but not axonal suffering, suggesting that, in *L-pgds*$^{-/-}$ mice, Schwann cells might not recognize the axon as intact despite NRG1 type III forward signaling. Whether the myelin damage is the result of myelin instability or the lack of continuous communication is currently unknown. We cannot exclude the possibility that L-PGDS exerts both functions. In future studies, it will be particularly important to determine how neuronal specific ablation of L-PGDS *in vivo* in adults affects myelin stability.

The use of agonists enhancing L-PGDS enzymatic activity, the transduction capability of Gpr44 or both could constitute a new approach to treating peripheral demyelinating neuropathies. Furthermore, as this pathway might be involved in myelin maintenance, activation of prostaglandins could be particularly efficacious for the treatment of demyelinating disorders with late onset. Notably, specific molecules that have already been developed and whose efficacy has been tested in other biological systems[36] are available and could pharmacologically target this level of communication between glial cells.

In conclusion, we propose that NRG1 type III controls myelination in multiple ways. The canonical forward signal is required to initiate myelination[31] and regulate the amount of myelin formed[50]. The backward signal, by upregulating the expression of L-PGDS, activates a previously unknown pathway that is relevant in PNS myelination and maintenance and whose modulation could be beneficial for the treatment of peripheral demyelinating neuropathies.

METHODS

Methods and any associated references are available in the online version of the paper.

Accession codes. The data discussed in this publication have been deposited in NCBI's Gene Expression Omnibus and are accessible through GEO Series accession number GSE61784.

Note: Any Supplementary Information and Source Data files are available in the online version of the paper.

ACKNOWLEDGMENTS

We thank V. Marzano and A. Urbani for shotgun mass spectrometry analyses, F. Clarelli for heat map and statistical analyses, G. Fitzgerald (University of Pennsylvania) for providing *Gpr44*$^{-/-}$ mice, P. Podini for excellent technical assistance with electron microscopy analyses, and P. Del Boccio for LC-MS/MS analyses. We are grateful to M. Buono, S. Previtali and A. Bolino for critical reading of the manuscript and suggestions, and L. Massimino for artwork. Part of this work was carried out in ALEMBIC, an advanced microscopy laboratory at the San Raffaele Scientific Institute. M.G.F. conducted this study in partial fulfillment for her Ph.D. in Molecular and Cellular Neuroscience, San Raffaele University. This study was supported by the Italian Minister of Health (award number GR08-35, C.T.), the European Marie Curie Reintegration Grant (award number IRG 239430-2008, C.T.) and the Agence Nationale pour la Recherche (ANR blanc programme, B.B.B.). C.T. is also supported by Italian Fondazione Italiana Sclerosi Multipla.

AUTHOR CONTRIBUTIONS

A.T. designed and conducted the majority of the experiments. M.G.F., V.A. and A.L. contributed to *in vitro* and biochemical studies. P.B. and F.M.B. performed expression studies. G.D. and A.Q. performed morphological and ultrastructural analyses. Y.U. and B.B.-B. provided transgenic lines and provided input. D.P. and P.S. performed the MS/MS-LC analyses. C.T. designed the experimental plan, supervised the project and wrote the manuscript.

COMPETING FINANCIAL INTERESTS

The authors declare competing financial interests: details are available in the online version of the paper.

1. Birchmeier, C. & Nave, K.A. Neuregulin-1, a key axonal signal that drives Schwann cell growth and differentiation. *Glia* **56**, 1491–1497 (2008).
2. Willem, M. *et al.* Control of peripheral nerve myelination by the beta-secretase BACE1. *Science* **314**, 664–666 (2006).
3. Hu, X. *et al.* Bace1 modulates myelination in the central and peripheral nervous system. *Nat. Neurosci.* **9**, 1520–1525 (2006).
4. La Marca, R. *et al.* TACE (ADAM17) inhibits Schwann cell myelination. *Nat. Neurosci.* **14**, 857–865 (2011).
5. Bao, J., Wolpowitz, D., Role, L.W. & Talmage, D.A. Back signaling by the Nrg-1 intracellular domain. *J. Cell Biol.* **161**, 1133–1141 (2003).
6. Bao, J. *et al.* Activity-dependent transcription regulation of PSD-95 by neuregulin-1 and Eos. *Nat. Neurosci.* **7**, 1250–1258 (2004).
7. Chen, Y., Hancock, M.L., Role, L.W. & Talmage, D.A. Intramembranous valine linked to schizophrenia is required for neuregulin 1 regulation of the morphological development of cortical neurons. *J. Neurosci.* **30**, 9199–9208 (2010).
8. Urade, Y. & Eguchi, N. Lipocalin-type and hematopoietic prostaglandin D synthases as a novel example of functional convergence. *Prostaglandins Other Lipid Mediat.* **68–69**, 375–382 (2002).
9. Giacomelli, S., Leone, M.G., Grima, J., Silvestrini, B. & Cheng, C.Y. Astrocytes synthesize and secrete prostaglandin D synthetase *in vitro*. *Biochim. Biophys. Acta* **1310**, 269–276 (1996).
10. Samy, E.T. *et al.* Sertoli cell prostaglandin D2 synthetase is a multifunctional molecule: its expression and regulation. *Endocrinology* **141**, 710–721 (2000).
11. Nagata, N. *et al. De novo* synthesis, uptake and proteolytic processing of lipocalin-type prostaglandin D synthase, beta-trace, in the kidneys. *FEBS J.* **276**, 7146–7158 (2009).
12. Tootle, T.L. Genetic insights into the *in vivo* functions of prostaglandin signaling. *Int. J. Biochem. Cell Biol.* **45**, 1629–1632 (2013).
13. Haskew-Layton, R.E., Payappilly, J.B., Xu, H., Bennett, S.A. & Ratan, R.R. 15-Deoxy-Delta12,14-prostaglandin J2 (15d-PGJ2) protects neurons from oxidative death via an Nrf2 astrocyte-specific mechanism independent of PPARgamma. *J. Neurochem.* **124**, 536–547 (2013).
14. Kerr, B.J., Girolami, E.I., Ghasemlou, N., Jeong, S.Y. & David, S. The protective effects of 15-deoxy-delta-(12,14)-prostaglandin J2 in spinal cord injury. *Glia* **56**, 436–448 (2008).
15. Urade, Y. & Hayaishi, O. Prostaglandin D synthase: structure and function. *Vitam. Horm.* **58**, 89–120 (2000).
16. Kostenis, E. & Ulven, T. Emerging roles of DP and CRTH2 in allergic inflammation. *Trends Mol. Med.* **12**, 148–158 (2006).
17. Beuckmann, C.T. *et al.* Cellular localization of lipocalin-type prostaglandin D synthase (beta-trace) in the central nervous system of the adult rat. *J. Comp. Neurol.* **428**, 62–78 (2000).
18. Kao, S.C. *et al.* Calcineurin/NFAT signaling is required for neuregulin-regulated Schwann cell differentiation. *Science* **323**, 651–654 (2009).
19. Grimwood, S. *et al.* Determination of guinea-pig cortical gamma-secretase activity *ex vivo* following the systemic administration of a gamma-secretase inhibitor. *Neuropharmacology* **48**, 1002–1011 (2005).

20. Beuckmann, C.T. *et al.* Lipocalin-type prostaglandin D synthase (beta-trace) is located in pigment epithelial cells of rat retina and accumulates within interphotoreceptor matrix. *J. Neurosci.* **16**, 6119–6124 (1996).
21. Mohri, I. *et al.* Prostaglandin D2–mediated microglia/astrocyte interaction enhances astrogliosis and demyelination in twitcher. *J. Neurosci.* **26**, 4383–4393 (2006).
22. Subra, C. *et al.* Exosomes account for vesicle-mediated transcellular transport of activatable phospholipases and prostaglandins. *J. Lipid Res.* **51**, 2105–2120 (2010).
23. Irikura, D. *et al.* Biochemical, functional, and pharmacological characterization of AT-56, an orally active and selective inhibitor of lipocalin-type prostaglandin D synthase. *J. Biol. Chem.* **284**, 7623–7630 (2009).
24. Vesin, M.F., Urade, Y., Hayaishi, O. & Droz, B. Neuronal and glial prostaglandin D synthase isozymes in chick dorsal root ganglia: a light and electron microscopic immunocytochemical study. *J. Neurosci.* **15**, 470–476 (1995).
25. Ragolia, L. *et al.* Accelerated glucose intolerance, nephropathy, and atherosclerosis in prostaglandin D2 synthase knock-out mice. *J. Biol. Chem.* **280**, 29946–29955 (2005).
26. Qu, W.M. *et al.* Lipocalin-type prostaglandin D synthase produces prostaglandin D2 involved in regulation of physiological sleep. *Proc. Natl. Acad. Sci. USA* **103**, 17949–17954 (2006).
27. Kanekiyo, T. *et al.* Lipocalin-type prostaglandin D synthase/beta-trace is a major amyloid beta-chaperone in human cerebrospinal fluid. *Proc. Natl. Acad. Sci. USA* **104**, 6412–6417 (2007).
28. Moniot, B. *et al.* The PGD2 pathway, independently of FGF9, amplifies SOX9 activity in Sertoli cells during male sexual differentiation. *Development* **136**, 1813–1821 (2009).
29. Raff, M.C., Abney, E., Brockes, J.P. & Hornby-Smith, A. Schwann cell growth factors. *Cell* **15**, 813–822 (1978).
30. Monje, P.V., Athauda, G. & Wood, P.M. Protein kinase A–mediated gating of neuregulin-dependent ErbB2-ErbB3 activation underlies the synergistic action of cAMP on Schwann cell proliferation. *J. Biol. Chem.* **283**, 34087–34100 (2008).
31. Taveggia, C. *et al.* Neuregulin-1 type III determines the ensheathment fate of axons. *Neuron* **47**, 681–694 (2005).
32. Ogata, T. *et al.* Opposing extracellular signal–regulated kinase and Akt pathways control Schwann cell myelination. *J. Neurosci.* **24**, 6724–6732 (2004).
33. Newbern, J.M. *et al.* Specific functions for ERK/MAPK signaling during PNS development. *Neuron* **69**, 91–105 (2011).
34. Lal, M. & Caplan, M. Regulated intramembrane proteolysis: signaling pathways and biological functions. *Physiology (Bethesda)* **26**, 34–44 (2011).
35. Harizi, H. The immunobiology of prostanoid receptor signaling in connecting innate and adaptive immunity. *Biomed. Res. Int.* **2013**, 683405 (2013).
36. Taketomi, Y. *et al.* Mast cell maturation is driven via a group III phospholipase A2-prostaglandin D2–DP1 receptor paracrine axis. *Nat. Immunol.* **14**, 554–563 (2013).
37. Tin, A. *et al.* Genome-wide significant locus of beta-trace protein, a novel kidney function biomarker, identified in European and African Americans. *Nephrol. Dial. Transplant.* **28**, 1497–1504 (2013).
38. Greenberg, M.E., Xu, B., Lu, B. & Hempstead, B.L. New insights in the biology of BDNF synthesis and release: implications in CNS function. *J. Neurosci.* **29**, 12764–12767 (2009).
39. Evans, S.F. *et al.* Neuronal brain-derived neurotrophic factor is synthesized in excess, with levels regulated by sortilin-mediated trafficking and lysosomal degradation. *J. Biol. Chem.* **286**, 29556–29567 (2011).
40. Nicholson, J.D. *et al.* PGJ(2) provides prolonged CNS stroke protection by reducing white matter edema. *PLoS ONE* **7**, e50021 (2012).
41. Kipanyula, M.J. *et al.* Calcineurin-nuclear factor of activated T cells regulation of Krox-20 expression in Schwann cells requires elevation of intracellular cyclic AMP. *J. Neurosci. Res.* **91**, 105–115 (2013).
42. Hirahara, Y. *et al.* G protein-coupled receptor 30 contributes to improved remyelination after cuprizone-induced demyelination. *Glia* **61**, 420–431 (2013).
43. Hennen, S. *et al.* Decoding signaling and function of the orphan G protein–coupled receptor GPR17 with a small-molecule agonist. *Sci. Signal.* **6**, ra93 (2013).
44. Monk, K.R. *et al.* A G protein–coupled receptor is essential for Schwann cells to initiate myelination. *Science* **325**, 1402–1405 (2009).
45. Monk, K.R., Oshima, K., Jors, S., Heller, S. & Talbot, W.S. Gpr126 is essential for peripheral nerve development and myelination in mammals. *Development* **138**, 2673–2680 (2011).
46. Glenn, T.D. & Talbot, W.S. Analysis of Gpr126 function defines distinct mechanisms controlling the initiation and maturation of myelin. *Development* **140**, 3167–3175 (2013).
47. Mogha, A. *et al.* Gpr126 functions in Schwann cells to control differentiation and myelination via G-protein activation. *J. Neurosci.* **33**, 17976–17985 (2013).
48. Ganfornina, M.D. *et al.* ApoD, a glia-derived apolipoprotein, is required for peripheral nerve functional integrity and a timely response to injury. *Glia* **58**, 1320–1334 (2010).
49. Comley, L.H. *et al.* ApoE isoform–specific regulation of regeneration in the peripheral nervous system. *Hum. Mol. Genet.* **20**, 2406–2421 (2011).
50. Michailov, G.V. *et al.* Axonal neuregulin-1 regulates myelin sheath thickness. *Science* **304**, 700–703 (2004).

ONLINE METHODS

Mice and genotyping. Generation of *H-pgds*$^{-/-}$; *L-pgds*$^{-/-}$ mice has been described previously[51,52]. *H-pgds*$^{-/-}$; *L-pgds*$^{-/-}$ mice were obtained in Mendelian ratio, by crossing *H-pgds*$^{+/-}$ and *L-pgds*$^{+/-}$ mice. All experiments were performed on animals of both sexes in a C57/Bl6 congenic background. Mice were genotyped by PCR using the following primers. Wild-type alleles: 5′-GAGTTGCTGCATCTGACCTTTTC-3′ and 5′-TAGCGAATAATTTCGG CTCTTCC-3′; *H-PGDS*: (773 bp) and 5′-TGTCAGGAATGTGGTATGCTC-3′ and 5′-AATACAGCTTTCTTCTCCCGGAAC-3′; *L-PGDS*: (338 bp) and the following PCR cycling conditions: 95 °C for 30 s, 52 °C for 30 s and 72 °C for 60 s (30 cycles). *H-PGDS*$^{-/-}$: 5′-ATCGCCTTCTATCGCCTTCTTGACGAGT-3′ and 5′-ATGTGTACTGGCTCCAACTTCCCAGAGAGT-3′ (800 bp); *L-PGDS*$^{-/-}$: 5′-TCTTGAGAGTGCAACAGAGCAAAGGAGTCC-3′ and 5′-ATCGCCTTCT ATCGCCTTCTTGACGAGT-3′ (650 bp) and the following PCR cycling conditions: 95 °C for 30 s, 60 °C for 30 s and 72 °C for 60 s (30 cycles).

Generation of *Gpr44*$^{-/-}$ has been previously described[53]. *Gpr44*$^{-/-}$ were genotyped by PCR using the following primers. 5′-CTCGCCGGACACGCT GAACTTGT-3′, 5′-TGGGGTCAAACTCAGCTCCTCACG-3′, and 5′-GCG GCGGCTAA CAAGTCGGATAG-3′ with the following PCR cycling conditions: 93 °C for 30 s, 55 °C for 30 s and 72 °C for 180 s (35 cycles). All amplified fragments were analyzed on a 1.5% agarose gel. All experiments involving animals followed protocols approved by the Animal Care and Use Committee of San Raffaele Scientific Institute.

Constructs. Full-length NRG1 type III lentivirus (pL6/V5 NRG1) was generated as described[31]. The C-NRG1 plasmid was obtained by cloning the *EGFP* cDNA in frame into the unique Xho I restriction site of pL6/V5 NRG1. *Nrg1* stop codon and *EGFP* ATG were mutated by standard PCR mutagenesis. N-NRG1 was obtained by standard PCR mutagenesis by cloning the *EGFP* sequence in frame and without its ATG between aminoacid 26 and 27 of NRG1 type III cDNA, to avoid interference with putative NRG1 signal peptide.

NRG1 ICD–EGFP was obtained by cloning the intracellular domain of rat NRG1 type III, from K 1020 to V 2100, without the stop codon, in the *pL6/V5* plasmid by topoisomerase. Upstream K1020 we inserted an ATG by standard PCR mutagenesis. The *EGFP* cDNA was cloned in frame into the unique Xho I restriction site of pL6/V5 NRG1-ICD. *Nrg1* stop codon and *EGFP* ATG were mutated by standard PCR mutagenesis.

NRG1 type III–FLAG and NRG1 ICD–FLAG plasmids were obtained by replacing the *EGFP* epitope into C-NRG1 and NRG1 ICD–EGFP with the 3XFLAG epitope. The 3XFLAG epitope was amplified by PCR from the p3X-FLAG-CMV-14 expression vector (Sigma Aldrich). Specifically, we introduced the XhoI and SacII restriction sites in the p3XFLAG-CMV-14 vector upstream and downstream the *3XFLAG* sequence respectively by PCR mutagenesis.

Rat *L-PGDS* cDNA was amplified by PCR from brain mRNA and cloned into the pL6/V5 plasmid in the Spe I and Sac II restriction sites. All constructs were obtained following standard molecular biology techniques and confirmed by sequencing.

Cell cultures. Mouse and rat DRG neurons were isolated from E14.5 or E16.5 embryos and established on collagen-coated glass coverslips as described[31]. Explants were cycled either with FUDR to eliminate all non–neuronal cells or in some experiments endogenous Schwann cells were maintained. Neuronal media was supplemented with 50 ng ml^{-1} NGF (Harlan, Bioproducts for Science). Primary rat Schwann cells were prepared as described[31] and maintained in DMEM (Invitrogen), 10% FBS (vol/vol, Invitrogen), 2 mM L-glutamine (Invitrogen), until used. Rat Schwann cells were added (200,000 cells per coverslip) to establish explant cultures of DRG neurons and myelination was initiated by supplementing media with 50 μg ml^{-1} ascorbic acid (Sigma–Aldrich).

In some experiments, purified DRG neurons, Schwann cell–DRG neuronal co-cultures or isolated Schwann cells were treated with various concentrations of AT-56 (Cayman Chemicals), 5, 10, 25 and 50 μM 15R-methyl-prostaglandin D2 (Cayman Chemicals), 10 μM Compound E (EMD Millipore) both dissolved in DMSO (Sigma Aldrich), 10 nM cyclosporin A (Novartis), 100 nM recombinant PGD2 dissolved in ethanol (Cayman Chemicals), 2.5 μM Forskolin (Sigma Aldrich), 2.5 ng ml^{-1} recombinant human NRG1β1 (EGF domain, R&D).

Lentiviral production and infection. Individual shRNA clones (TRCN0000027873: shA3; TRCN0000027876: shA5; TRCN0000027894: shC9) specifically targeting mouse *Gpr44* were obtained through the RNAi Consortium (Open Biosystem/Thermoscientific). Lentiviral vectors, *Gpr44* shRNA and scramble shRNA were transfected into 293FT cells (Invitrogen) and viruses were produced as described[4]. Viral supernatants were collected and stored as described[4]. Freshly plated Schwann cells (10^6 cells per 100-mm plate) were incubated for 2 d with *Gpr44* shRNA lentiviruses at a 2/3 dilution (vol/vol) in DMEM, 10% FBS and 2 mM D-glutamine supplemented with forskolin and rh NRG-1 (EGF domain, R&D). Cells were expanded for an additional week and maintained for 3 d in Schwann cell media prior seeding. Protein knockdowns were confirmed by qRT-PCR analyses. Mouse and rat DRG neuronal explants were infected the day after the dissection and left in the presence of the virus for 24 h after which cultures were purified of endogenous Schwann cell to obtain pure DRG neurons by cycling them with antimitotic reagents or cultured with endogenous Schwann cell. In the latter case, both DRG neurons and mouse primary Schwann cell were infected.

Electron microscopy and morphological analyses. Semi-thin and ultrathin sections were obtained as described[54]. Tissues were removed and fixed with 2% glutaraldehyde (vol/vol) in 0.12 M phosphate buffer, postfixed with 1% osmium tetroxide (vol/vol), and embedded in Epon (Fluka). Semi-thin sections (0.5–1 μm thick) were stained with toluidine blue and examined by light microscopy (Olympus BX51). Ultrathin sections (70–90 nm thick) were stained with uranile acetate and lead citrate and examined by electron microscopy (Leo 912 Omega). Digitized non-overlapping semi-thin sections images from corresponding levels of the sciatic nerve were obtained with a digital camera (Leica DFC300F) using a 100× objective. *g* ratio measurements were performed on digitized non overlapping electron micrographs images. *g* ratio was determined by dividing the mean diameter of an axon without myelin by the mean diameter of the same axon with myelin. A minimum of 150 randomly chosen fibers per animal were analyzed for *g* ratio measurements at P7, 1 month, 2 months, 6 months, 8 months and 9 months. To determine the size distribution of myelinated fibers in sciatic nerves, diameters of all fibers in at least ten images of randomly chosen representative images were measured and binned based on their width. All measurements were acquired on electron microscopy sections images using an ImageJ software. Data are expressed as the percentage relative to the total number of fibers. Similarly, the number of myelinated fibers per area in sciatic nerves and roots was determined on 100× images acquired on semi-thin sections and analyzed using ImageJ Software. All measurements were blindly performed. Electron microscopy analyses on Schwann cell–DRG neurons myelinating co-cultures were performed as described previously[55].

Microarray analyses. Gene expression study was performed using the Illumina RatRef-12 Expression BeadChips. Each individual array on the chip targets more than 21,000 transcripts selected primarily from the NCBI RefSeq database (Release 16) and in a minor part from the UniGene database. 500 ng of total RNA was reverse transcribed into cRNA (complementary RNA) and biotin-UTP labeled using the Illumina TotalPrep RNA Amplification Kit (Ambion). 750 ng of cRNA in 11 μl (150 ng μl^{-1}) were hybridized to the BeadChip Array at 58 °C overnight. The fluorescent signal was developed through a streptavidin-Cy3 staining step. BeadChips were imaged using the Illumina BeadArray Reader, a two-channel 0.8-μm resolution confocal laser scanner. The software Illumina GenomeStudio version 2011.1 was used to take fluorescent hybridization signals and to assess the system quality controls, such as biological specimen, hybridization, signal generation and negative controls. For each experimental condition four biological replicates have been analyzed, and technical replicates have been tested in 4 of 12 samples. The mean correlation coefficient value of technical replicates was 0.993 (s.d., 0.005) and of biological ones was 0.967 (s.d., 0.013). Sample clustering analysis based on the absolute correlation metric parameter was also performed, and the graphical representation of the dendrogram further supported the technical validity of the data.

Data were $\log_2$ transformed, normalized using the quantile algorithm (R beadarray package) and all probes with a detection $P > 0.01$ in all experimental conditions were excluded from the analyses. For differential expression analysis, a moderated *t* statistics was performed using Limma package in R. Fold change values were also calculated. Transcript probes were classified as differentially

expressed based on a fold change cut-off of 2.0 and $P < 0.01$ considering the following comparisons: lentiviruses expressing NRG1 ICD versus not infected; lentiviruses expressing *EGFP* versus not infected and lentiviruses expressing *NRG1 ICD* versus those expressing only *EGFP*.

Microarray data were deposited in Array Express with the following accession number: E-MTAB-2131. The data discussed in this publication have been deposited in NCBI's Gene Expression Omnibus and are accessible through GEO Series accession number GSE61784.

RNA isolation and measurements. Total RNA was isolated from rat Schwann cells, rat purified DRG neurons and co-cultures using Trizol (Roche), according to manufacturer's instruction. Total RNA was retro-transcribed to cDNA as described[56]. Aliquots of RT products were tested in parallel using primers pair for rat *L-pgds* and *Gapdh*. *L-pgds* primers were: 5′-GAGAAGAAAGAG CTACTGTTTATGTGC-3′ (forward) and 5′-CTAAAGGTGATGAATTTCTC CTTCAG-3′ (reverse). PCR cycling conditions were 94 °C for 30 s, 56 °C for 60 s and 72 °C for 90 s, 24 cycles, followed by 5 min extension at 72 °C. *Gapdh* primers were: 5′-GGTTACCAGGGCTGCCTTCTCTTGTGA-3′ (forward) and 5′-CGGAAGGGGCGGAGATGATGACCCT-3′ (reverse). PCR cycling conditions were: 94 °C for 30 s, 64 °C for 60 s and 72 °C for 90 s, 22 cycles, followed by 5 min extension at 72 °C.

qRT-PCR. PCR analyses were performed using Sso Fast Eva Green Supermix according to manufacturer's instructions. Genes of interest and housekeeping genes were amplified using the same reaction protocol. To test *L-PGDS*, *Nfatc4* and *Sod3* expression we used the following set of primers: *L-pgds*: 5′-GAGAAGAAAGAGCTACTGTTTATGTGC-3′ (forward) and 5′-CTAA AGGTGATGAATTTCTCCTTCAG-3′ (reverse); *Nfatc4* 5′-CAGGTCTACT TTTTATGTCTCCAATGG-3′ (forward) and 5′-ATCCGTAGGCCAGATCT ATAAGACG-3′ (reverse); *Sod3* 5′–TTCTTGTTCTGCAACCTGCTACT-3′ (forward) and 5′-ATTGAAGGAGGCCTCAAGTCTG-3′ (reverse); *Gapdh*: 5′-GGTCTACATGTTCCAGTATGACTCTA-3′ (forward) and 5′-CTTCTTG AGGGAGTTGTCATATTTCTC-3′ (reverse). PCR cycling conditions were 95 °C for 30 s, 56 °C for 60 s 72 °C for 90 s (41 cycles). To test *Ptgdr*, *Pparg* and *Gpr44* expression we used the following primers: *Ptgdr*: 5′-CA TTCTCGGTAATAGGCTTCTCTG-3′ (forward) and 5′-TCCACAAGTTTA AAGGCTCCATAG-3′ (reverse); *Pparg*: 5′-CTGTCGGATCCACAAAAA GAGTAG (forward) and 5′-GAATTCATGTCGTAGATGACAAATG-3′ (reverse); *Gpr44*: 5′-CACTACTCTATGTGCTCACTTGTCC-3′ (forward) and 5′-CCATCTAATCCAAAGTACAGCTCAA-3′ (reverse); *Gapdh*: 5′-ACCTCA ACTACATGGTCTACATGTTC-3′ (forward) and 5′-ATCTTGAGGGAGTT GTCATATTTCTC-3′ (reverse). PCR cycling conditions were: 95 °C for 30 s, 58 °C for 60 s, 72 °C for 90 s (41 cycles).

To determine *L-pgds* expression in mouse DRG–rat Schwann cell co-cultures, we used the primers specific for the mouse sequence that do not amplify the rat gene. *L-pgds*: 5′-GGAGAAGAAAGCTGTATTGTATATGTGC-3′ (forward); 5′-TAAAGGTGGTGAATTTCTCCTTCAG-3′ (reverse); *Gapdh*: 5′-TCACCAGGGCTGCCATTTGCAGTGG-3′ (forward) 5′-CGGAAGGGGC GGAGATGATGACCCT-3′ (reverse). PCR cycling conditions were: 95 °C for 30 s, Tm for 60 s, 72 °C for 60 s (41 cycles). Tm was for 56 °C mouse *L-pgds* and 62 °C for mouse *Gapdh*.

LC-MS/MS analyses. Levels of PGD2 were measured by modifying previously described methods[57] by using a LC-MS/MS system (Waters). Briefly, after adjustment of sample to pH 3 with HCl 2N and incubation with methyloxamine HCl (1 g ml^{-2}) and d_6-PGE-M (40 ng), as internal standard, Cayman Chemical) for 60 min at 25 °C, PGD2 was extracted by using Strata-X 33-μm polymeric reversed phase SPE columns (30 mg ml^{-1}, Phenomenex) and eluted with ethyl acetate and then dried with a Speed-Vac (Speed Vac Plus, Savant Instruments). After dryness, the pellet was resuspended with 50 μl of water/ACN (90/10) and injected into a LC-MS/MS system. The LC-MS/MS system consisted into a Waters Alliance 2795 LC coupled to a Micromass Quattro Pt triple-quadrupole mass spectrometer (TQuattro-Pt, Waters) equipped with a Z-Spray ESI source, operated in negative ion mode. The LC column was a Synergy HydroRP (150 × 1 mm, 4μ) (Phenomenex) maintained at 25 °C. The mobile phase was acetonitrile (solvent A) and water (solvent B) (both added with 0.005% acetic acid, vol/vol) at a flow rate of 0.070 ml min^{-1}.

The gradient timetable was the following: injection at 10% A; 70% A at 25 min; 10% A at 26 min; 10% A at 40 min. The ionization mode was electrospray in negative polarity (ES). The transitions monitored in Multiple Reaction Monitoring (MRM) are 380>186 *m/z* for the endogenous compound PGD2 and 391>342 *m/z* for the internal standard PGEMd6. The collision energy used was 14 eV.

Preparation of detergent lysates and immunoblotting. Tissues and cell lysates were prepared as described[31]. Supernatants were aliquoted and stored at −80 °C until used. Protein concentrations were determined by the BCA method (Pierce); samples (20–40 μg of protein) were fractionated by SDS-PAGE and blotted onto nitrocellulose (Protran Biosciences). Membranes were blocked in 5% BSA, 0.05% sodium azide in TBST (0.1% Triton X-100 in Tris-buffered saline (TBS), vol/vol). Appropriate regions were excised, incubated with specific primary and secondary antibodies, washed in TBST and developed with the SuperSignal chemiluminescent substrate (Pierce). For quantitative western blotting analyses, filters were analyzed using the Odyssey Infrared Imaging System (LI-COR Biosciences) according to manufacturer's instructions.

Tunel and proliferation assays. Both assays were performed as described[58] on three different P2 mice per genotype and four different slides per animal. For proliferation assays, sciatic nerve sections were permeabilized with 0.2% Triton X-100 (vol/vol), blocked with 10% FCS (vol/vol), 0.1 M lysine, and 0.02% sodium azide (vol/vol) in 0.1 M phosphate-buffered saline (PBS), and incubated with a rabbit antibody to PH3 (Millipore). Tunel assay was performed on adjacent sections using the DeadEnd Fluorometric TUNEL System (Promega G3250) according to manufacturer's instructions.

Antibodies and immunofluorescence. All antibodies used were previously validated for the applications used, except for antibody to L-PGDS, which we validated in lysates prepared from *L-pgds*$^{-/-}$ mice, and antibody to H-PGDS, which we confirmed on sciatic nerve cryosections of *H-pgds*$^{-/-}$ mice. Mouse monoclonal antibodies included antibodies to MBP (Covance SMI-94R and SMI-99R, 1:4,000 for western blotting), neurofilament (Covance SMI-31R and SMI-32R, 1:10,000 for western blotting), neuronal class III β-tubulin (TuJ1, Covance MMS-435 1:1,000 for immunofluorescence) and Caspr (NeuroMab clone K65/35, 1:100 for immunohistochemistry). Rabbit polyclonal antibodies included antibodies to actin (Sigma Aldrich A2066, 1:5,000 for western blotting), FLAG (Sigma Aldrich F7425, 1:400 for immunohistochemistry), Calnexin (Sigma-Aldrich, C4731 1:4,000 for western blotting), L-PGDS (Abnova PAB 12054, 1:500 for western blotting), H-PGDS (LSBio LS-B6886/48259, 1:200 for immunofluorescence), S100 beta (DakoCytomation Z0311, 1:200 for immunofluorescence), phospho-AKT (ser 473) (Cell Signaling Technology 4060, 1:1,000 for western blotting), total AKT (Cell Signaling Technology 4691, 1:1,000 for western blotting), phospho-ERK (p44, p42) (Cell Signaling Technology 9101, 1:1,000 for western blotting), total ERK (Cell Signaling Technology 9102, 1:1,000 for western blotting), Nfat3 (Cell Signaling Technology 2183, 1:500 for western blotting), phospho-PKA (Cell Signaling Technology 5661, 1:1,000 for western blotting), total PKA (Cell Signaling Technology 4782, 1:1,000 for western blotting), Calcineurin B1 (Cell Signaling Technology 2614, 1:1,000 for western blotting), cleaved caspase-3 (Cell Signaling Technology 9661, 1:200 for immunofluorescence), p-Histone H3 (EMD Millipore 06-570, 1:500), Egr2 (1:1000 for immunohistochemistry) and Pou3f1 (1:100 for immunohistochemistry), both a generous gift from D. Mejier (University of Edinburgh). Chicken antibodies include antibodies to neurofilament M (Covance PKC-593P, 1:2,000 for immunohistochemistry), MPZ (Millipore AB9352, 1:500 for western blotting), GFP (Abcam 13970, 1:1,000 for immunohistochemistry). Rat MBP hybridoma (diluted 1:2 in immunohistochemistry) was a generous gift from V. Lee (University of Pennsylvania).

Secondary antibodies included DyLight 549 (Jackson ImmunoResearch 715-505-150, 1: 500 for immunohistochemistry), DyLight 488 (Jackson ImmunoResearch 703-485-155, 1:500 for immunohistochemistry), goat antibody to rabbit HRP (Jackson ImmunoResearch 111-035-003, 1:5.000 for western blotting). Infrared secondary antibodies for quantitative western blotting analyses were obtained from LI-COR Biosciences and all used 1:10,000 (goat antibody to mouse IRDye 680 926-68070; goat antibody to mouse IRDye 800 926-68070; goat antibody to rabbit IRDye 680 926-68021; goat antibody to rabbit IRDye 800 926-32211). Co-cultures were fixed in and permeabilized in 100% methanol at −20 °C for 15 min, stained and examined as described[31]. Sciatic nerves

were dissected from P2 mice and immediately fixed in 4% paraformaldehyde (vol/vol) in 0.1 M 1× PBS at +4 °C, cryo-protected in 20% sucrose (Sigma-Aldrich), embedded in OCT (Miles), and snap-frozen in liquid nitrogen. Sections were stained as described[58] and examined by epifluorescence on a Leica DM 4500 microscope and by confocal microscopy on a Leica SP5.

Statistical analyses. No statistical assays were used to pre-determine the sample size. Nonetheless, we chose samples of comparable size, especially to perform *in vitro* experiments. Data were collected randomly and assessed blindly. The data distribution was assumed to be normal, although we did not formally test it. Limma method used in the microarray differential expression analysis is based on an estimate of variance, which is moderated across genes[59]. All statistical analyses were performed on at least three different experiments. Statistical detailed analyses are reported in each figure legends and all assays (two sided Fischer's exact test, one-way ANOVA Dunnett's multiple comparison test, two sided moderate *t* test and two tailed unpaired *t* test) were performed using the Prism Software package (GraphPad).

A **Supplementary Methods Checklist** is available.

51. Eguchi, N. *et al.* Lack of tactile pain (allodynia) in lipocalin-type prostaglandin D synthase-deficient mice. *Proc. Natl. Acad. Sci. USA* **96**, 726–730 (1999).
52. Trivedi, S.G. *et al.* Essential role for hematopoietic prostaglandin D2 synthase in the control of delayed type hypersensitivity. *Proc. Natl. Acad. Sci. USA* **103**, 5179–5184 (2006).
53. Nelson, A.M. *et al.* Prostaglandin D2 inhibits wound-induced hair follicle neogenesis through the receptor, Gpr44. *J. Invest. Dermatol.* **133**, 881–889 (2013).
54. Quattrini, A. *et al.* Beta 4 integrin and other Schwann cell markers in axonal neuropathy. *Glia* **17**, 294–306 (1996).
55. Bolis, A. *et al.* Dlg1, Sec8 and Mtmr2 regulate membrane homeostasis in Schwann cell myelination. *J. Neurosci.* **29**, 8858–8870 (2009).
56. Wrabetz, L. *et al.* A minimal human MBP promoter-lacZ transgene is appropriately regulated in developing brain and after optic enucleation, but not in shiverer mutant mice. *J. Neurobiol.* **34**, 10–26 (1998).
57. Song, W.L., Lawson, J.A., Wang, M., Zou, H. & FitzGerald, G.A. Noninvasive assessment of the role of cyclooxygenases in cardiovascular health: a detailed HPLC/MS/MS method. *Methods Enzymol.* **433**, 51–72 (2007).
58. Pellegatta, M. *et al.* alpha6beta1 and alpha7beta1 integrins are required in Schwann cells to sort axons. *J. Neurosci.* **33**, 17995–18007 (2013).
59. Smyth, G. K. Linear models and empirical bayes methods for assessing differential expression in microarray experiments. *Stat. Appl. Genet. Mol. Biol.* **3**, 3 (2004).

Erratum: Prostaglandin D2 synthase/GPR44: a signaling axis in PNS myelination

Amelia Trimarco, Maria Grazia Forese, Valentina Alfieri, Alessandra Lucente, Paola Brambilla, Giorgia Dina, Damiana Pieragostino, Paolo Sacchetta, Yoshihiro Urade, Brigitte Boizet-Bonhoure, Filippo Martinelli Boneschi, Angelo Quattrini & Carla Taveggia
***Nat. Neurosci.*; doi:10.1038/nn.3857; corrected online 17 November 2014**

In the version of this article initially published online, a *P* value was incorrect on p. 5, first full paragraph. It read "We found similar alterations in 6-month-old sciatic nerves of *L-pgds*$^{-/-}$ mice, although the difference was not significant ($P = 0.649$; **Supplementary Table 2**)." The correct *P* value is 0.0649. Also, the first Results subheading read "NRG1 type III is cleaved and activates L-PGDS by γ-secretase"; it should have read "NRG1 type III is cleaved by γ-secretase and activates L-PGDS." The errors have been corrected for the print, PDF and HTML versions of this article.

Physical Medicine and Rehabilitation - International

Open Access

Austin Publishing Group

Case Report

Gait Training for Becker's Muscular Dystrophy Using Robot Suit Hybrid Assistive Limb

Asai T[1], Ojima I[1], Minami S[1], Takeshima Y[2] and Matsuo M[1,3]*

[1]Department of Physical Therapy, Kobegakuin University, Japan

[2]Department of Pediatrics, Hyogo College of Medicine, Japan

[3]Kobe University, Japan

*Corresponding author: Matsuo M, Department of Physical Therapy, Kobegakuin University, Japan, Tel: +81-78-974-2461; Fax: +81-78-974-2461; Email: mmatsuo@reha.kobegakuin.ac.jp

Received: October 03, 2014; **Accepted:** October 12, 2014; **Published:** October 14, 2014

Abstract

Becker's muscular dystrophy (BMD) is an X-linked recessive inherited disorder characterized by a slow and degenerative muscle weakness of the legs and pelvis. The patients eventually use walking aids or are wheelchair-bound in daily life because of the progression of disability. The robot suit hybrid assistive limb (HAL) is a new robot suit designed to assist voluntary control of lower limb motion by detecting extremely weak bioelectric signals on the skin surface. Here we report how HAL gait training can be adapted for a wheelchair-bound patient with BMD. A 25-year-old patient with BMD participated in HAL gait training.Gait training consisted of three phases: phase 1, adaptation of HAL for the patient; phase 2 (1 year), treadmill training with the body-weight supported walker (BWSW); and phase 3 (2 years), gait training on the floor with the BWSW. The subject completed 2 h of HAL gait training once a week (from August 2011 to August 2014). Although there are no standard exercises for patients with BMD, his gait ability and fitness improved, following HAL gait training. This result indicates that HAL gait training can be both feasible and safe when used as a part of a regular rehabilitation program for patients with BMD. Harness use seems to be essential for safety and feasibility of HAL gait for patients with BMD. The combined use of the HAL gait training and BWSW may be an effective rehabilitation tool for patients with BMD.

Keywords: Becker's muscular dystrophy; Hybrid assistive limb; Gait exercise; Body-weight supported walker

Introduction

Becker's muscular dystrophy (BMD) is an X-linked recessive inherited disorder, characterized by a slow and progressive degenerative muscle weakness of the legs and pelvis. Severity of the disease may markedly vary depending on the age of the patient at disease onset [1]. The patients eventually use walking aids or are wheelchair-bound in daily life because of progression of disability [2]. Rehabilitation exercises differ for ambulatory and wheelchair-bound patients. Gait training, activities of daily living (ADL) exercises and conventional physical therapy (stretching and range of motion at the lower limb joints) are practiced for ambulatory patients. Once patients become wheelchair-bound, gait training is no longer practiced; rehabilitation efforts instead focus on ADL exercises to maximize independent living.

The robot suit hybrid assistive limb (HAL) is a new robot suit designed to assist voluntary control of the knee and hip joint motion by detecting extremely weak bioelectric signals on the surface of the skin [3-5]. The HAL can support the wearer's lower limb motion while walking by adjusting the supportive level [3]. The HAL gait training is being increasingly employed for patients suffering from acquired neurological disease, such as stroke or spinal cord disease [4-9]. However, no studies have attempted to examine the feasibility of HAL rehabilitation for patients with BMD. Here we report a case in which the patient was wheelchair-bound and rehabilitation gait training had ceased. We report how HAL gait training can be adapted for use by a wheelchair-bound patient with BMD. Gait ability was influenced by HAL training.

Case Presentation

A 25-year-old patient with BMD (height, 164 cm; weight, 54 kg) participated in HAL gait training. He was diagnosed with BMD by dystrophin immune-staining of biopsied muscle tissue at 9 years of age because of the appearance of motor function deficits [10]. After the onset of BMD symptoms, his physical function gradually declined, and he began using a wheelchair outdoors at the age of 15. At the age of 22, walking was no longer possible. From the age of 23, he participated in conventional physical therapy, including muscle strength and range of motion exercises, twice a week in preparation for HAL gait training. At the age of 25, he started HAL gait training in addition to conventional physical therapy. Prior to participating in HAL gait training, the subject provided informed consent; the study was approved by the Ethics Committee of the Kobegakuin University (HEB121211-1).

Mode Setting of HAL

The HAL has a hybrid control system consisting of Cybernic Voluntary Control (CVC) and Cybernic Autonomous Control (CAC) [9]. The CVC supports the patient's voluntary lower limb motion according to the voluntary muscle activity and assistive torque provided to each joint. In this study, we used the CVC, which allows the operator to adjust the degree of physical support to the patient's comfort. In addition, the HAL has two modes, walking mode and stand up mode, which support voluntary movement of walking and standing up, respectively, according to the electrical signals of muscle contracture and load on the feet. In this study, we used the walking

Citation: Asai T, Ojima I, Minami S, Takeshima Y and Matsuo M. Gait Training for Becker's Muscular Dystrophy Using Robot Suit Hybrid Assistive Limb. Phys Med Rehabil Int. 2014;1(3): 4.

Table 1: Summary of gait training.

Phase 1 Adaptation of HAL suit for patient	Phase 2 (1 year) Treadmill training with BWSW	Phase 3 (2 years) Gait training on the floor with BWSW
• Search for the body parts to detect the bioelectrical signal for hip extension. • Apply the special harness to BWSW.	• 2 h of training once a week (gait training: 1 h). • The treadmill speed was adjusted to patient's condition (0.6–1.6 km/h) • The gait speed of the treadmill and the walking distance during training increased (the distance that the patient walked before the heart rate reached 125 bpm).	• 2 h of training once a week (gait training: 1 h) • Walking speed was adjusted by a therapist to pull the BWSW but not exceeding the heart rate of 125 bpm. • Walking distance during training increased (the distance that the patient walked before the heart rate reached 125 bpm). • 5 times sit-to-stand exercise after gait training

mode for gait training and stand up mode for sit-to-stand exercises. Furthermore, we monitored the heart rate during gait training to ensure that the working load was safe and appropriate.

Training

Gait training consisted of three phases: phase 1, adaptation of HAL for the patient; phase 2, treadmill training with the body-weight supported walker (BWSW); and phase 3, gait training on the floor with the BWSW. Typical gait training (phases 1 and 2) proceeded as follows: attaching electrodes, wearing the HAL and harness, and setting up the computer (45 min); HAL gait training (60 min, including rest time); removing the HAL and harness (15min). In phase 3, five sit-to-stand exercises (5STS) were added after gait training. All gait trainings and 5 STS were conducted by three physical therapists. The training phase is summarized in Table 1.

Phase 1: Adaptation of HAL suit for the patient

According to the manufacturer's instructions, electrodes for the hip extension were attached just below the ischial tuberosity. However, sufficient electrical signals of muscle contraction were not detected in this area. Several electrodes were placed on different sites around the hip joints, and an area on the upper part of the gluteus maximus muscle was found to enable bioelectrical signal detection (Figure 1). When applying the HAL, we used BWSW to adjust the working load (Figure 2). BWSW is a modified body support system, which has been used for the HAL gait training for patients with stroke and spinal cord injury [9, 11]. A HAL supplier-recommended special harness in the BWSW was used for the patient (Figure 3A). We were able to adjust the height of patient from the floor using a handle on the outside of the frame (Figure 3B). In addition, this system can be set up to be used with a treadmill or as a special walker on the floor (Figure 4, 5).

Phase 2: Treadmill training with BWSW

In this phase, the subject under went 2 h of HAL gait training once a week for 1 year (Figure 4). The treadmill speed was adjusted to the patient's condition. The subject could not continue walking with HAL so much after his heart rate reached at 125 bpm. For the safety reason, 125 bpm was set as the discontinuance criteria for the HAL gait training. The treadmill speed and walking distance during the training was the speed and distance before his heart rate reached at 125 bpm, and they were gradually increased (Figure 6). We started with a treadmill speed of 0.6 km/hr and walking distance of 200 meters, because he felt the difficulty of walking with HAL in the begining and his heart rate reached at 125 bpm very easily. Near the end of phase 2, the subject could walk at a speed of 1.6 km/h and walk a distance of >700 meters. Additionally, the subject walked on the treadmill with 1-3° incline in the last 100 meters when his condition was good. His average heart rate was approximately 110 bpm during walking.

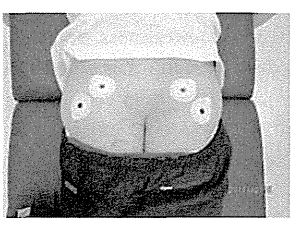

Figure 1: Locations of electrodes for hip extension.

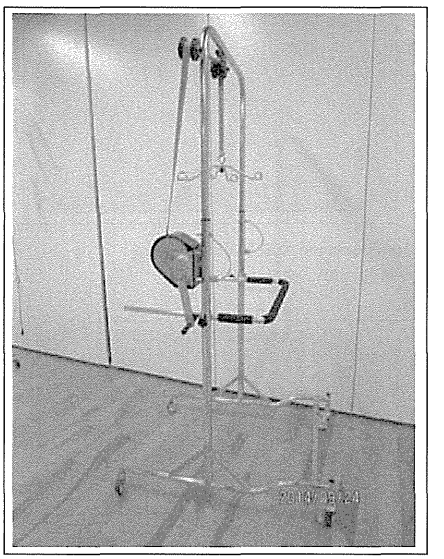

Figure 2: Body-weight supported walker.

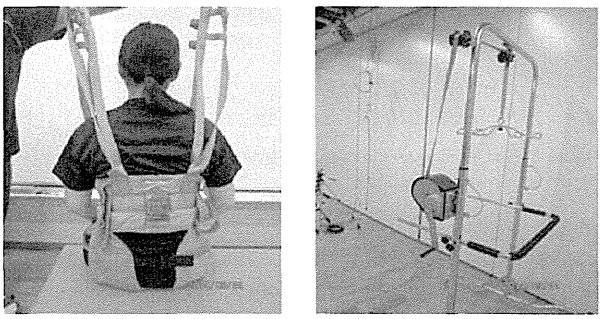

A: The harness for gait training

B: Handle for the adjustment of patient height

Figure 3: Treadmill training with the BWSW with harness.
BWSW: body-weight supported walker
A: The harness for gait training,
B: Handle for the adjustment of patient height

Phase 3: Gait training on the floor using the BWSW

After phase 2, we began gait training on the floor (Figure 5).

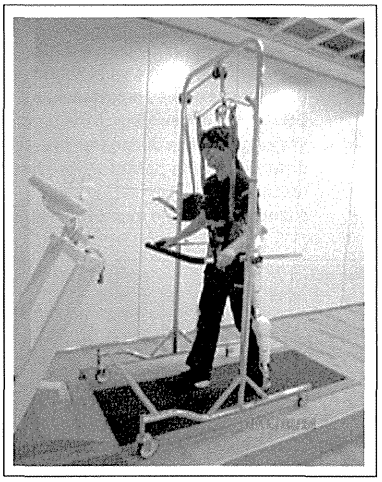

Figure 4: Treadmill training with BWSW.
BWSW: body-weight supported walker.

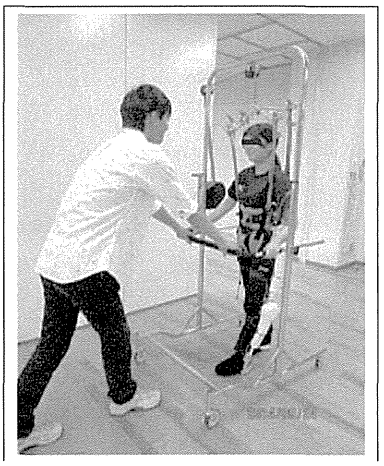

Figure 5: Gait training on the floor with BWSW.
BWSW: body-weight supported walker.

Walking speed was adjusted by a therapist to pull the BWSW but not exceed a heart rate of 125 bpm. The initial walking distance during training was less than 200 meters, but it was gradually increased to approximately 500 meters (Figure 6). After gait training and some rest, 5STS was performed. Three therapists helped the subject stand up on a platform, which was 50 cm above the floor. One therapist was in front to manually support him stand up, and the other two assisted from the sides to pull up the harness. His heart rate frequently reached 125 bpm during the last 5STS trial. When his heart rate reached 125 bpm before the last trial, we stopped the exercise immediately. Clinical assessments were performed at the initial evaluation and 3 years after HAL gait training (Table 2).

Discussion

This case report describes the feasibility of HAL gait training for patients with BMD. In general, patients with neuromuscular disease do not undergo gait training during the non-ambulatory phase [12]. This patient had not undergone gait training since he had become wheelchair-bound. Although there are no standard exercises for patients with BMD or severe Duchenne muscular dystrophy [13], his

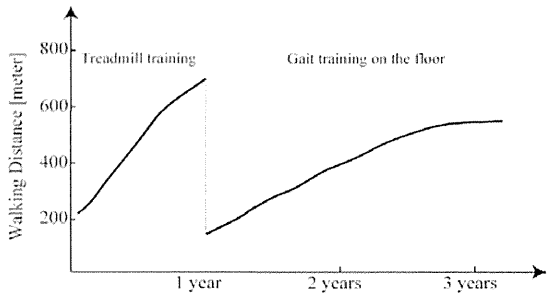

Figure 6: The time course of walking distance during gait training.
Walking distance: The distance that the patient walked during training before his heart rate reached 125 bpm.

Table 2: Results of clinical assessments.
BMI, body mass index; ROM, range of motion; R/L, Right/Left; MMT, manual-muscle testing.

	Pre-training (initial evaluation)	Post-training (3 years later)
Body weight (kg)	56	54
BMI	20.8	20.1
ROM (°)		
Hip extension (R/L)	−30/−20	−25/−20
Knee extension (R/L)	−20/−15	−20/−15
Ankle dorsiflexion(R/L)	−25/−25	−25/−20
MMT		
Hip extension (R/L)	2−/2−	2−/2−
Knee extension (R/L)	2−/2−	2−/2−
Shoulder flexion (R/L)	2/2	2/2
Shoulder extension (R/L)	2/2	2/2
Elbow extension (R/L)	3/3	3/3
Brook upper extremity scale	2	2
Vignos lower extremity scale	9	9

gait ability and fitness improved with HAL gait training. This finding indicates that HAL gait training is both feasible and safe when used as a part of a regular rehabilitation program for patients with BMD.

All gait trainings were performed using BWSW, which provided safety and gait speed control. The combined use of the HAL and BWSW is important for HAL gait training in patients with BMD. The combination allowed the patient to stop walking whenever he wanted. Although the BWSW height occasionally limited the reduction of weight load, it was satisfactory in the present case. The use of a harness seems essential to allow safe HAL gait training for patients with BMD.

The HAL training began long after the patient became wheelchair-bound. HAL gait training at an early phase may be necessary to prevent lower limb muscle weakness or joint contracture due to disuse syndrome as described in other conditions [9]. In the present case, the training frequency was relatively limited (once a week, Table 1). Furthermore, other physical exercises, such as knee extension exercise with HAL, were not performed. Other physical functions, such as muscle strength and range of motion, may be recovered by additional HAL trainings. Finally, improvement was not observed in the clinical assessment (Table 2). Other medication should be

combined with HAL gait training to achieve clinical improvement. Further study is needed in this area.

Conclusion

For patients with BMD, HAL gait training may be an effective rehabilitation tool.

Acknowledgment

The authors would like to thank Enago (www.enago.jp) for the English language review.

References

1. Emery AE, Skinner R . Clinical studies in benign (Becker type) X-linked muscular dystrophy. Clin Genet. 1976; 10: 189-201.
2. Emery AE . The muscular dystrophies. Lancet. 2002; 359: 687-695.
3. Kawamoto H, Sankai Y: Power assist method based on Phase Sequence and muscle force condition for HAL.Adv Robot2005, 19: 717-734.
4. Maeshima S, Osawa A, Nishio D, Hirano Y, Takeda K, Kigawa H,et al . Efficacy of a hybrid assistive limb in post-stroke hemiplegic patients: a preliminary report. BMC Neurol. 2011; 11: 116.
5. Sakakima H, Ijiri K, Matsuda F, Tominaga H, Biwa T, Yone K, et al: A newly developed robot suit hybrid assistive limb facilitated walking rehabilitation after spinal surgery for thoracic ossification of the posterior longitudinal ligament: a case report.Case Rep Orthop 2013, 2013: 621405.
6. Kubota S, Nakata Y, Eguchi K, Kawamoto H, Kamibayashi K, Sakane M, et al . Feasibility of rehabilitation training with a newly developed wearable robot for patients with limited mobility. Arch Phys Med Rehabil. 2013; 94: 1080-1087.
7. Kawamoto H, Kamibayashi K, Nakata Y, Yamawaki K, Ariyasu R, Sankai Y, et al . Pilot study of locomotion improvement using hybrid assistive limb in chronic stroke patients. BMC Neurol. 2013; 13: 141.
8. Ueba T, Hamada O, Ogata T, Inoue T, Shiota E, Sankai Y . Feasibility and safety of acute phase rehabilitation after stroke using the hybrid assistive limb robot suit. Neurol Med Chir (Tokyo). 2013; 53: 287-290.
9. Nilsson A, Vreede KS, Häglund V, Kawamoto H, Sankai Y, Borg J . Gait training early after stroke with a new exoskeleton - the hybrid assistive limb: a study of safety and feasibility. J Neuroeng Rehabil. 2014; 11: 92.
10. Takeshima Y, Yagi M, Okizuka Y, Awano H, Zhang Z, Yamauchi Y, et al: Mutation spectrum of the dystrophin gene in 442 Duchenne/Becker muscular dystrophy cases from one Japanese referral center.J Hum Genet 2010, 55: 379-388.
11. Aach M, Cruciger O2, Sczesny-Kaiser M3, Höffken O3, Meindl RC2, Tegenthoff M3, et al . Voluntary driven exoskeleton as a new tool for rehabilitation in chronic spinal cord injury: a pilot study. Spine J. 2014; .
12. Bushby K, Finkel R, Birnkrant DJ, Case LE, Clemens PR, Cripe L, et al . Diagnosis and management of Duchenne muscular dystrophy, part 1: diagnosis, and pharmacological and psychosocial management. Lancet Neurol. 2010; 9: 77-93.
13. Bushby K, Finkel R, Birnkrant DJ, Case LE, Clemens PR, Cripe L, et al . Diagnosis and management of Duchenne muscular dystrophy, part 2: implementation of multidisciplinary care. Lancet Neurol. 2010; 9: 177-189.

Citation: Asai T, Ojima I, Minami S, Takeshima Y and Matsuo M. Gait Training for Becker's Muscular Dystrophy Using Robot Suit Hybrid Assistive Limb. Phys Med Rehabil Int. 2014;1(3): 4.